

 Open access • Journal Article • DOI:10.1038/S41593-018-0168-3

## Direct pericyte-to-neuron reprogramming via unfolding of a neural stem cell-like program — [Source link](#)

Marisa Karow, Marisa Karow, J. Gray Camp, Sven Falk ...+17 more authors

**Institutions:** Ludwig Maximilian University of Munich, University of Mainz, Max Planck Society, University of Naples Federico II ...+2 more institutions

**Published on:** 18 Jun 2018 - Nature Neuroscience (Nature Publishing Group)

**Topics:** Reprogramming, SOX2, Neural stem cell, Neural development and Cellular differentiation

Related papers:

- [Direct conversion of fibroblasts to functional neurons by defined factors](#)
- [In vivo direct reprogramming of reactive glial cells into functional neurons after brain injury and in an Alzheimer's disease model.](#)
- [Identification and Successful Negotiation of a Metabolic Checkpoint in Direct Neuronal Reprogramming](#)
- [Dissecting direct reprogramming from fibroblast to neuron using single-cell RNA-seq](#)
- [Reprogramming of Pericyte-Derived Cells of the Adult Human Brain into Induced Neuronal Cells](#)

Share this paper:    

View more about this paper here: <https://typeset.io/papers/direct-pericyte-to-neuron-reprogramming-via-unfolding-of-a-4ux95i2l6y>

# Direct pericyte-to-neuron reprogramming via unfolding of a neural stem cell-like program

Marisa Karow<sup>1,2,13\*</sup>, J. Gray Camp<sup>3,13</sup>, Sven Falk<sup>2,4</sup>, Tobias Gerber<sup>3</sup>, Abhijeet Pataskar<sup>5</sup>, Malgorzata Gac-Santel<sup>3</sup>, Jorge Kageyama<sup>3</sup>, Agnieszka Brazovskaja<sup>3</sup>, Angela Garding<sup>5</sup>, Wenqiang Fan<sup>1</sup>, Therese Riedemann<sup>2</sup>, Antonella Casamassa<sup>1,12</sup>, Andrej Smiyakin<sup>6</sup>, Christian Schichor<sup>7</sup>, Magdalena Götz<sup>2,4</sup>, Vijay K. Tiwari<sup>5</sup>, Barbara Treutlein<sup>3,8,9,14\*</sup> and Benedikt Berninger<sup>1,10,11,14\*</sup>

**Ectopic expression of defined transcription factors can force direct cell-fate conversion from one lineage to another in the absence of cell division. Several transcription factor cocktails have enabled successful reprogramming of various somatic cell types into induced neurons (iNs) of distinct neurotransmitter phenotype. However, the nature of the intermediate states that drive the reprogramming trajectory toward distinct iN types is largely unknown. Here we show that successful direct reprogramming of adult human brain pericytes into functional iNs by *Ascl1* and *Sox2* encompasses transient activation of a neural stem cell-like gene expression program that precedes bifurcation into distinct neuronal lineages. During this transient state, key signaling components relevant for neural induction and neural stem cell maintenance are regulated and functionally contribute to iN reprogramming and maturation. Thus, *Ascl1*- and *Sox2*-mediated reprogramming into a broad spectrum of iN types involves the unfolding of a developmental program via neural stem cell-like intermediates.**

Direct lineage reprogramming is an emerging strategy for harnessing the cellular plasticity of differentiated cells for lineage conversion into desired target cell types for disease modeling and tissue repair<sup>1–4</sup>. While direct lineage reprogramming from starting to target-cell type classically occurs without cell division, thereby sharply contrasting with reprogramming toward induced pluripotency<sup>5</sup>, little is known about the intermediate states that bridge the trajectory between start and end points. Two models have been proposed, according to which direct reprogramming is mediated either through direct conversion between fully differentiated states or through reversal to a developmentally immature state<sup>6</sup>. Furthermore, reprogramming efficiency and final differentiation outcomes are highly cellular-context-dependent, for which the underlying reasons are only incompletely understood<sup>7,8</sup>. Analyses of the transcriptome alterations induced by the reprogramming factors have yielded fundamental insights into the molecular mechanisms of iN conversion<sup>9–12</sup>. For instance, a single factor, *Ascl1*, can reprogram mouse astrocytes into iNs with high efficiency<sup>13</sup>, while the same factor induces a muscle cell-like fate in mouse embryonic fibroblasts (MEF) alongside neuronal fates<sup>11,14</sup>. Efficient reprogramming of MEFs into iNs requires co-expression of additional factors (for example, *Brn2*, *Ascl1* and *Myl1l*, collectively referred to as BAM)<sup>9,11,12,15</sup>. Moreover, *Ascl1* induces a GABAergic neuron identity in mouse astrocytes<sup>10,13</sup>, while BAM-transduced fibroblasts predominantly adopt a glutamatergic phenotype<sup>15</sup>, raising questions of how the respective reprogramming

trajectories translate into distinct iN transmitter and subtype identities.

In the present study, by analyzing transcriptomes at population and single cell level, we aimed to reconstruct the trajectories underlying direct lineage conversion of adult human brain pericytes into iNs by forced expression of *Ascl1* and *Sox2* (AS)<sup>16</sup>. This allowed us to scrutinize the contribution of the starting cell population's heterogeneity to the variability in reprogramming success. By identifying cells of distinct reprogramming competence, we were able to reconstruct a trajectory of productive AS-mediated iN generation, allowing us to uncover intermediate states during successful conversion. Unexpectedly, we found that despite the absence of cell division, cells in the productive trajectory passed through a neural stem cell-like state. Transiently induced genes, many of which are core components of signaling pathways, typified this intermediate state, and interference with these signaling pathways demonstrated their functional importance for the reprogramming process. Finally, the productive reprogramming trajectory revealed an unexpected point of bifurcation into lineages whose transcriptomes were dominated by transcription factor families involved in the specification of GABAergic and glutamatergic subclasses of forebrain neurons.

## Results

***Ascl1* and *Sox2* synergism in inducing neuronal gene expression in pericytes.** We have recently shown that adult human brain pericytes can be reprogrammed into iNs via forced expression of the

<sup>1</sup>Institute of Physiological Chemistry, University Medical Center Johannes Gutenberg University Mainz, Mainz, Germany. <sup>2</sup>Physiological Genomics, Biomedical Center, Ludwig Maximilians University Munich, Planegg/Martinsried, Germany. <sup>3</sup>Max Planck Institute for Evolutionary Anthropology, Leipzig, Germany. <sup>4</sup>Institute for Stem Cell Research, Helmholtz Center Munich, German Research Center for Environmental Health, Neuherberg, Germany. <sup>5</sup>Institute of Molecular Biology (IMB), Mainz, Germany. <sup>6</sup>Miltenyi Biotec GmbH, Bergisch Gladbach, Germany. <sup>7</sup>Department of Neurosurgery, Ludwig Maximilians University, Munich, Germany. <sup>8</sup>Max Planck Institute of Molecular Cell Biology and Genetics, Dresden, Germany. <sup>9</sup>Technical University Munich, Munich, Germany. <sup>10</sup>Focus Program Translational Neuroscience, Johannes Gutenberg University Mainz, Mainz, Germany. <sup>11</sup>Centre for Neurodevelopmental Biology, Institute of Psychiatry, Psychology & Neuroscience, King's College London, London, UK. <sup>12</sup>Present address: Division of Pharmacology, School of Medicine, "Federico II" University of Naples, Naples, Italy. <sup>13</sup>These authors contributed equally: Marisa Karow, J.Gray Camp. <sup>14</sup>These authors jointly supervised this work: Barbara Treutlein, Benedikt Berninger. \*e-mail: [marisa.karow@med.uni-muenchen.de](mailto:marisa.karow@med.uni-muenchen.de); [barbara\\_treutlein@eva.mpg.de](mailto:barbara_treutlein@eva.mpg.de); [berningb@uni-mainz.de](mailto:berningb@uni-mainz.de)

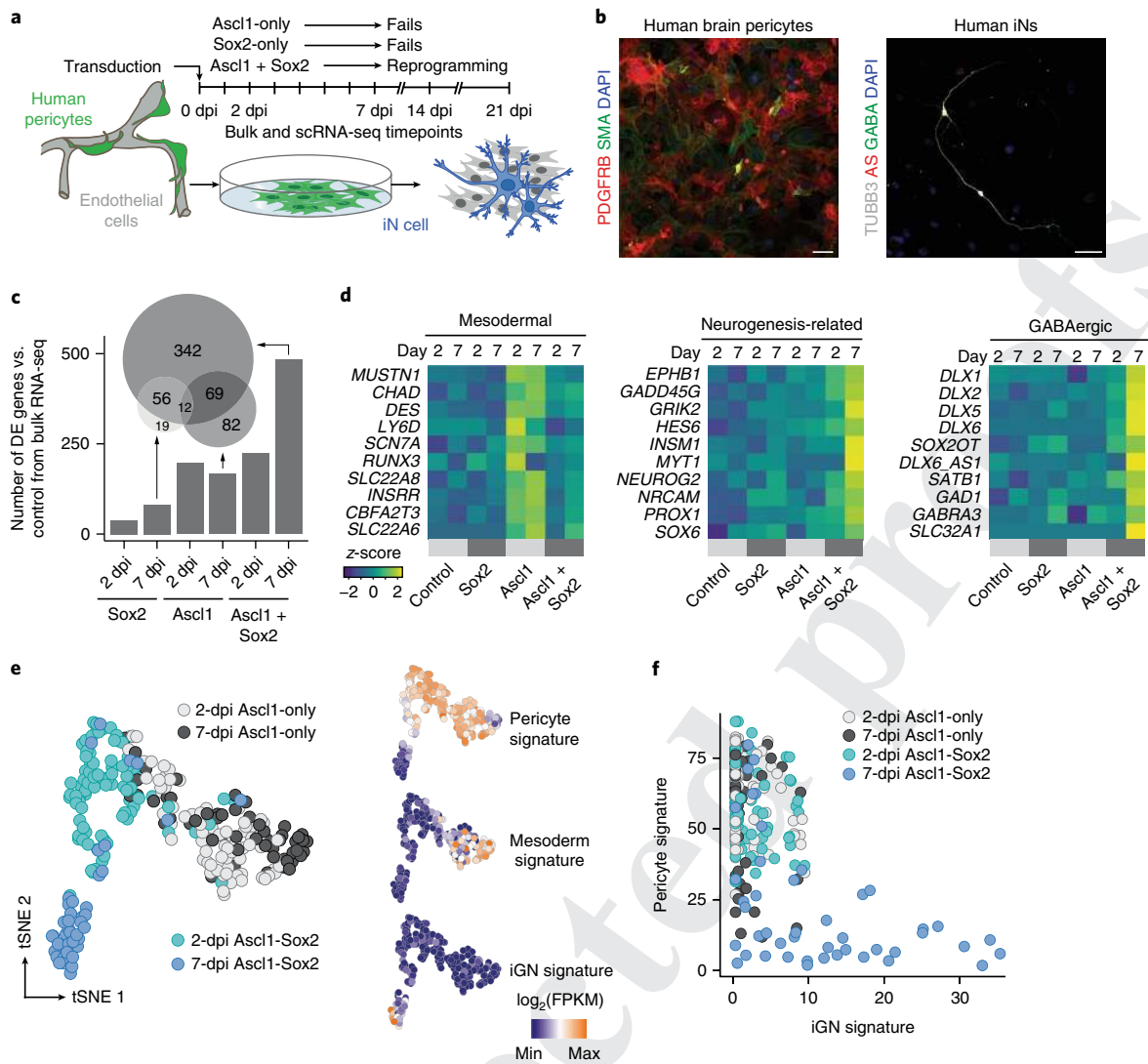


**Fig. 1 | Ascl1-Sox2 synergism is required for pericyte-to-iN reprogramming.** **a**, Schematic of experiments in this figure. Cells expressing Ascl1 and/or Sox2 are fluorescently labeled and isolated by fluorescence-activated cell-sorting (FACS) for bulk and scRNA-seq analyses at indicated timepoints following transduction. **b**, Representative micrographs of cultured human pericytes expressing pericyte markers PDGFRB and SMA, before (left) and after transformation (right) into TUBB3<sup>+</sup> and GABA<sup>+</sup> iNs by overexpressing AS at 46 dpi ( $n > 30$ ). Nuclei are stained with DAPI. Scale bar, 50  $\mu$ m. **c**, Bulk RNA-seq with pericytes derived from three individual donors was performed at 2 and 7 dpi with Ascl1-only, Sox2-only, or AS. Bar graph shows the number of differentially expressed (DE) genes (adjusted  $P$  value ( $P_{adj}$ )  $< 0.01$ ; calculated according to Benjamini-Hochberg) in each condition compared to pericytes transduced with a control vector. The Euler diagram shows the overlap of the DE genes at 7 dpi. Note that the majority of DE genes results from AS synergism. **d**, Heatmaps show normalized expression (z-score) of representative DE genes highlighting the induction of mesodermal, neurogenesis-related, and GABAergic signature genes at both 2 and 7 dpi. **e**, scRNA-seq was performed at 2 and 7 dpi on cells transduced with Ascl1-only ( $n = 82$  cells at 2 dpi and 64 cells at 7 dpi) and AS ( $n = 86$  cells at 2 dpi and 48 cells at 7 dpi). Principal component analysis (PCA; calculated on a total of 280 cells) followed by t-SNE shows that the pericyte signature is diminished in many 7-dpi Ascl1-only and strongly diminished in the majority of 7-dpi AS cells, concomitant with the acquisition of a mesoderm and GABAergic neuron (iGN) signature in Ascl1-only and AS-cells, respectively. Signatures were calculated by summing the expression of the fate-determinants highlighted in **d** (Supplementary Table 5). **f**, The iGN signature is plotted for all Ascl1-only and AS cells relative to the pericyte signature.

transcription factors Ascl1 and Sox2, and time-lapse imaging showed that this conversion occurs in the absence of cell division, qualifying it as direct lineage reprogramming<sup>16</sup>. Given that adult human brain pericyte reprogramming into functional iNs requires co-expression of Sox2 alongside Ascl1<sup>16</sup>, we first addressed the contribution of each factor individually or in combination with the gene expression programs underlying pericyte-to-neuron conversion (Fig. 1a,b). We performed RNA-seq of early-passage cultured human brain pericytes, obtained from three different adult donors and transduced with retroviruses encoding a reporter for control, Ascl1, Sox2, or AS at early stages (2 d postinfection (dpi) and 7 dpi) of reprogramming

(Fig. 1a). Unexpectedly, Sox2 only induced minor changes in gene expression, at both 2 and 7 dpi (Fig. 1c, Supplementary Fig. 1a,e, and Supplementary Table 1). In contrast, Ascl1 and AS substantially altered gene expression at both stages (Fig. 1c and Supplementary Fig. 1a,e,f). Notably, Ascl1 and AS changed the expression of distinct sets of genes. We noticed that several of the Ascl1-only altered genes are expressed in cells of the mesodermal lineage, indicative of a failure to cross the lineage barrier toward neurogenesis. In sharp contrast, AS resulted in significant induction of genes related to neurogenesis (Fig. 1d, and Supplementary Fig. 1e,f, and Supplementary Table 1). Moreover, we detected upregulation of

several transcription factors and noncoding RNAs playing key roles in forebrain GABAergic neurogenesis<sup>17,18</sup> (Fig. 1d, Supplementary Fig. 1e,f, and Supplementary Tables 1 and 2). Yet we also observed a significant increase in *NEUROG2* expression (Fig. 1d), which is associated with diverse excitatory neuron identities.

Comparison of the genes upregulated by *Ascl1*-only or by AS with those transactivated by *Ascl1* in mouse neural stem cells<sup>19</sup> revealed a progressive induction of direct *Ascl1* neural stem cell target genes between 2 and 7 dpi (Supplementary Fig. 1b and Supplementary Table 3). However, many of the direct *Ascl1* neural stem cell target genes became induced only upon co-expression of *Sox2* (Supplementary Fig. 1c,d), indicating that the proposed on-target pioneer factor activity of *Ascl1*<sup>9,19</sup> is highly context-dependent.

To further dissect the differences in the early gene expression programs induced by *Ascl1* or AS, we measured 280 single-cell transcriptomes of *Ascl1*- ( $n = 146$ ) and AS-expressing ( $n = 134$ ) cells by single-cell RNA-seq at 2 and 7 dpi. Principal component analysis followed by *t*-stochastic neighbor embedding (t-SNE) of single-cell transcriptomes revealed an early and progressive separation of *Ascl1*-only and AS-expressing cells (Fig. 1e). Pericyte identity genes (for example, *PDGFRB*, *COL1A1*, and *CAV1*) became downregulated in *Ascl1*- and AS-expressing cells (Supplementary Fig. 1g), but only the latter acquired a GABAergic neuron fate signature (*DLX1/2*, *DLX5/6*, *SATB1*, etc.; Fig. 1e and Supplementary Fig. 1h). In agreement with our bulk RNA-seq data and published data from MEF-to-neuron reprogramming<sup>11</sup>, *Ascl1*-expressing cells induced myocyte differentiation genes (for example, *MUSTN1*; Supplementary Fig. 1h). Occasionally, individual AS cell transcriptomes clustered with those of *Ascl1*-only cells, suggesting failed AS synergism as a potential mechanism underlying reprogramming failure (Fig. 1f). Overall, these data demonstrate that *Ascl1* alone is unable to induce a neuronal program in adult human brain pericytes but requires synergism with *Sox2*.

### Pericyte heterogeneity and reprogramming competence.

To define the competence of adult human brain pericytes for AS-induced reprogramming, we next compared the transcriptomes of control pericytes with those of AS-transduced cells at early and later stages of reprogramming. To our surprise, t-SNE analysis revealed that control cells fell into two discernible clusters (Fig. 2a,b and Supplementary Fig. 2a,b), here referred to as group 1 and group 2 pericytes, with differentially enriched gene ontology terms (Supplementary Fig. 2c and Supplementary Table 4). While both groups highly expressed several classical pericyte genes (i.e., *PDGFRB*, *CAV1*, *DCN*, etc.; Fig. 2a and Supplementary Fig. 2b), other pericyte-associated genes such as *ANGPT1*, *APOE*, and *LEPR* were differentially expressed (Supplementary Fig. 2a,b), and such differential expression could be confirmed on the protein level (Fig. 2c,f and Supplementary Fig. 2d). Notably, transcriptomes of AS-transduced cells exhibited distinct degrees of relatedness to the two pericyte starting populations, with cells undergoing successful reprogramming being more similar to group 2 pericytes (Fig. 2d,e). These data strongly suggest that the two pericyte groups differed markedly in their response to AS. In fact, t-SNE analysis indicated that productive reprogramming toward neurogenesis originated specifically from group 2 pericytes (Fig. 2a,e). In contrast, group 1 pericytes appeared to give rise to a distinct population positive for the hypothalamic neuronal marker *PMCH* but lacking expression of other neuronal genes, which thus precluded identifying these cells as hypothalamic neurons (Fig. 2a). Besides AS-transduced cells clustering differentially with group 1 and group 2 pericytes, we observed two smaller clusters of AS-transduced cells enriched in genes involved in cell-cycle progression (for example, *MKI67*) and potentially an alternative fate marked by the expression of *POU2F3*. To independently corroborate differential neurogenic competence of group 1 and group 2 pericytes, we used fluorescence-activated

cell sorting to purify these populations via antibodies specific to the leptin receptor, encoded by the *LEPR* gene (Fig. 2f,g and Supplementary Fig. 2a,b). Consistent with the observation that iNs may originate from group 2 pericytes, we found that leptin-receptor-negative cells were more prone to undergo AS-induced neurogenesis than leptin-receptor-positive cells (Fig. 2h). These data provide experimental evidence that the two pericyte starter populations display distinct degrees of reprogramming competence.

**Transient activation of a neural stem cell-like program.** We next reconstructed the transcriptome trajectory of reprogramming-competent pericytes into iNs by pseudotemporal ordering<sup>20</sup> (Fig. 3a). Genes that mark pericyte identity, such as *PDGFRB*, *CAV1*, and *CFH*, became gradually downregulated. Conversely, genes associated with the acquisition of a neuronal fate were progressively upregulated with more linear (for example, *CHD7* and *DLX5*) or nonlinear dynamics (for example, *SNAP25*; Fig. 3b,c), possibly reflecting distinct gene expression waves during early and later phases of neuronal differentiation. Notably, we identified a set of genes that became upregulated early during the reprogramming process, but then declined again as neuronal differentiation progressed (Fig. 3b,c). We refer to these genes as 'switch genes'. These include genes involved in the regulation of cell signaling such as *NOG*, *LEFTY2*, *DKK1*, and *NOTCH2*, suggesting that modulation of signaling pathways is important during early phases of productive reprogramming (see below). The conspicuous dynamics of the regulation of these genes urged us to interrogate their expression during mouse embryonic development. Notably, the switch genes were markedly enriched in the germinal zones of the developing CNS containing the neural stem cells (Fig. 3d and Supplementary Fig. 3a). This strongly suggests that cells undergoing productive reprogramming by AS transiently acquire a neural stem cell-like state. This was further corroborated when analyzing the expression levels of these genes in human fetal brain tissue<sup>21</sup>, where higher levels of expression were found in distinct human neural stem cells (i.e., apical and basal radial glia) as compared to neurons (Fig. 3e). Consistent with the upregulation of the switch genes during successful reprogramming, mapping the switch gene signature onto the t-SNE plot shown in Fig. 2a revealed its specific occurrence in the cell population that connects productive group 2 pericytes with iNs (Fig. 3f). In contrast, the switch gene signature was absent from transcriptomes of AS-transduced cells in the immediate neighborhood of group 1 pericytes (Fig. 3f), indicating that acquisition of a neural stem cell like-state is critical for AS-mediated pericyte-to-iN reprogramming. Of note, mapping the same switch gene signature onto previously published single-cell transcriptomes undergoing MEF-to-iN reprogramming<sup>11</sup> revealed an unexpectedly high base level of switch gene expression in the MEF starting population, and its expression did not increase at any stage along the MEF-to-neuron axis but was found to be strongly decreased in neurons (Supplementary Fig. 3b). These data are indicative of fundamental differences in the reprogramming trajectories of these two distinct reprogramming pathways. Notably, time-lapse imaging of pericytes during AS reprogramming revealed the occurrence of different cellular morphologies: while at early phases of reprogramming, cells displayed a flat, fibroblast-like morphology, at subsequent phases, processes undergoing dynamic turnover akin to multipolar progenitors appeared (Fig. 3g and Supplementary Video 1). Finally, at the end of the reprogramming process, neuron-like cells dramatically decreased their motility and protruded processes of increased stability. Thus, the cellular behavior and morphology are consistent with the notion of distinct cellular states underlying the reprogramming of pericytes into iNs.

**Modulation of signaling pathways.** The conspicuous regulation of several components of signaling pathways known to play key



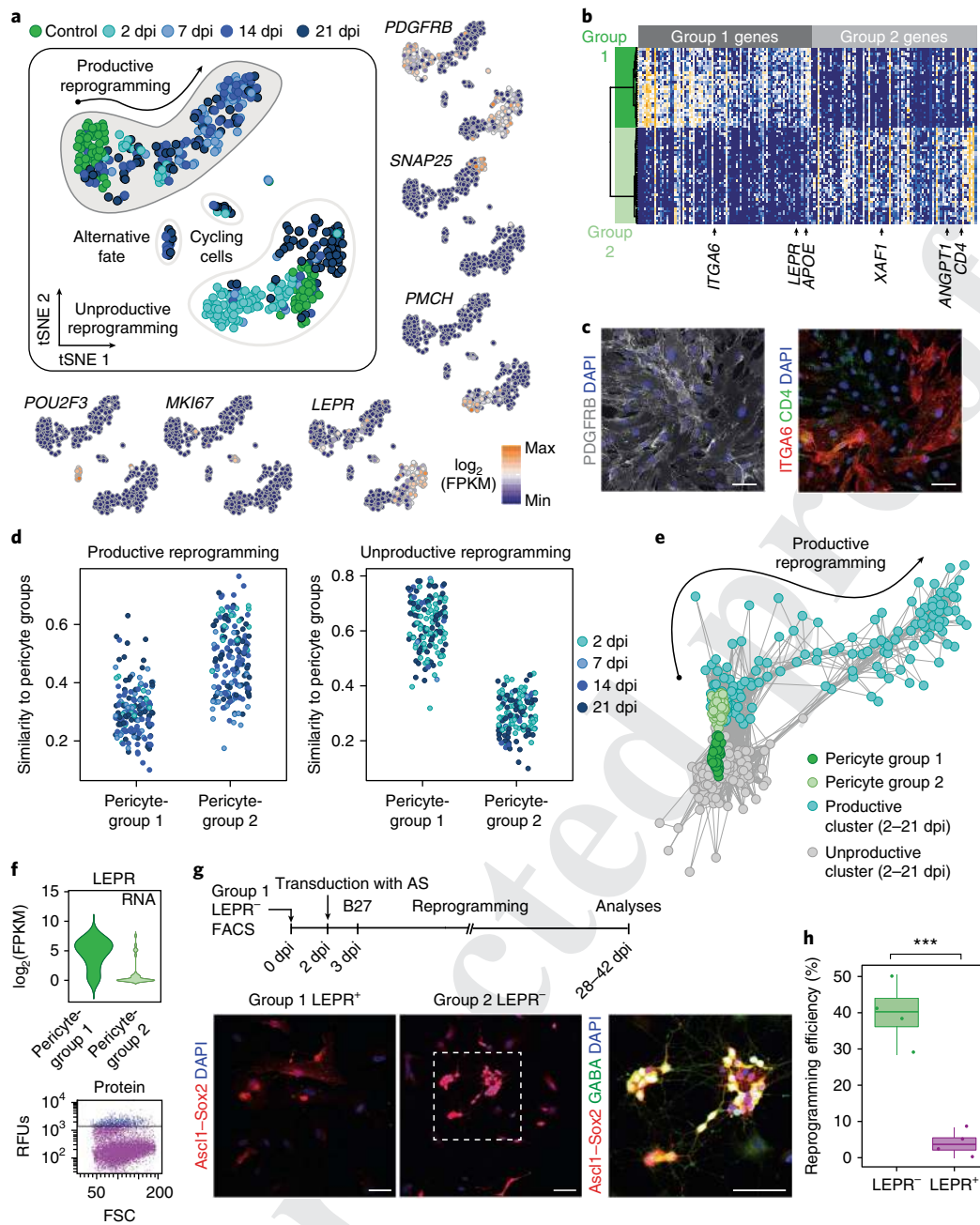


**Fig. 2 | Pericyte heterogeneity correlates with distinct reprogramming competence.** **a**, PCA (total of 419 cells) followed by t-SNE reveals heterogeneity during iN reprogramming, with genes marking distinct clusters colored on the adjacent t-SNE plots. Control-transduced pericytes (green) segregate into two distinct clusters. One cluster links to cells that express iN fate determinants (productive), whereas the other cluster is unlinked to iN reprogramming (unproductive). Cells expressing *MKI67* and other hallmarks of cycling cells are observed, as well as a group of cells expressing *POU2F3*. **b**, Heatmap shows the expression of genes that correlate with PC1 from PCA on control pericytes only. Hierarchical clustering reveals two distinct groups of pericytes with selected genes indicated below the heatmap. **c**, Left: micrographs showing cultured human brain pericytes stained against the pan-pericyte marker PDGFRB. Right: the same field of view of cultured human brain pericytes stained against pericyte group 1 marker ITGA6 and pericyte group 2 marker CD4. Nuclei are stained with DAPI ( $n = 3$  individual pericyte donors; two independent experiments). Scale bar, 50  $\mu\text{m}$ . **d**, Cells from the productive reprogramming cluster in **a** have a higher similarity to group 2 pericytes, while cells from the unproductive reprogramming clusters have a higher similarity to group 1 pericytes. **e**, Lineage network based on pairwise correlations between cells suggests that group 2 pericytes (lighter green population) are more competent to contribute to productive iN reprogramming. **f**, Top: violin blots show the density distribution of RNA expression of *LEPR* in pericyte groups 1 (31 cells) and 2 (44 cells). Bottom: representative flow cytometry plots show *LEPR* expression in cultured human brain pericytes (four independent experiments). **g**, Human brain pericytes were sorted based on *LEPR* expression (group 1 marker), plated, and transduced with AS to induce lineage conversion. Micrographs show AS-transduced pericytes at 35 dpi, with inset showing higher magnification of reprogrammed pericytes that acquired neuronal morphology and GABA immunoreactivity ( $n = 4$ ). Nuclei are stained with DAPI. Scale bars, 50  $\mu\text{m}$ . **h**, Quantification of reprogramming efficiency (dots represent independent individual experiments;  $n = 4$ ; data are represented as boxplots with whiskers; two-tailed unpaired Student's  $t$  test;  $***P = 0.000593$ ) reveals that the *LEPR*<sup>-</sup> pericyte subpopulation is more competent to iN reprogramming using AS, confirming predictions from scRNA-seq. Boxplots show median, quartiles (box), and range (whiskers).

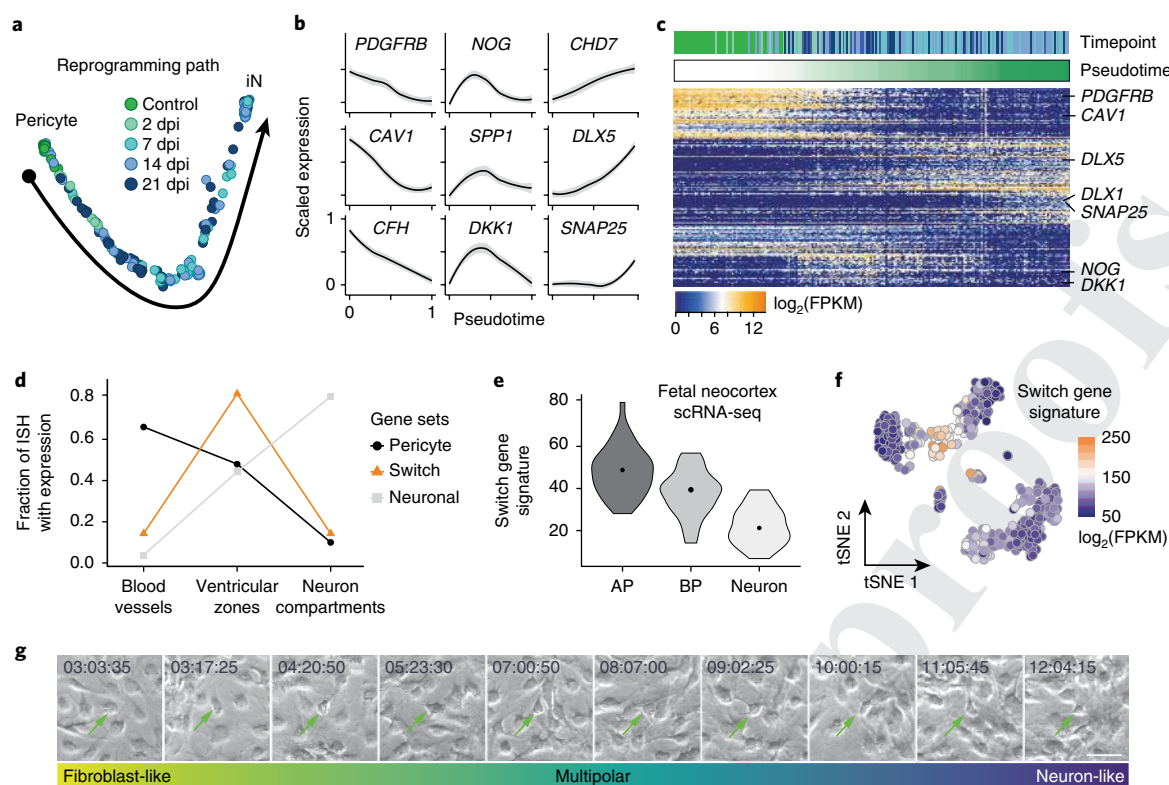


**Fig. 3 | A transient neural precursor-like state emerges on the reprogramming path to iNs. a**, PCA was performed on 211 single-cell transcriptomes from the productive reprogramming cluster shown in Fig. 2a. Monocle2 was used to infer a pseudotemporal ordering of cells. **b**, Scaled expression of representative marker genes in all 211 cells of the productive reprogramming path shown as a function of pseudotime. Shaded gray represents 95% confidence interval. **c**, Heatmap shows the expression of genes identified by PCA and ordered by hierarchical clustering. Cells are ordered according to pseudotime. The reprogramming path is characterized by three phases of gene expression changes. In the first phase, genes associated with pericyte identity are downregulated, concomitant with a transient upregulation of switch genes (for example, *NOG* and *DKK1*). In the second phase, genes associated with iN fate determination are upregulated (for example, *DLX5*). In the third phase, neuron maturation factors (for example, *DLX1* and *SNAP25*) are upregulated alongside phase 2 genes. **d**, Chart shows fraction of pericyte, switch, and neuronal genes (from **c**) expressed in blood vessels and meninges, ventricular zones, or neuron compartments determined from in situ patterns in the developing mouse brain. **e**, Violin plots show the density distribution of the switch gene signature from scRNA-seq of fetal human cortex (dots within the violins represent medians). Cortex cells are grouped based on cell type (41 apical progenitor cells (AP); 19 basal progenitor cells (BP); 42 early-born neurons (Neuron)). **f**, Switch gene signatures projected onto the t-SNE plot from Fig. 2a shows the induction of switch genes at an intermediate stage exclusively within the productive reprogramming path. **g**, Time-lapse imaging of AS-transduced cells over time (three independent experiments) shows the morphological changes during successful pericyte-to-neuron reprogramming (timepoints specified within the images). Arrows indicate a successfully reprogrammed pericyte throughout the different morphological changes mentioned below the images. Scale bar, 50  $\mu\text{m}$ .

roles during neural induction and neural stem cell maintenance<sup>22</sup>, such as the BMP inhibitor *NOG*, the *ACTIVIN/NODAL* inhibitor *LEFTY2*, and *NOTCH2* and its downstream targets *HEY1* and *ID1*, prompted us to investigate whether these pathways are of functional importance for successful reprogramming. To test the importance of modulation of *NODAL* and *BMP* signaling, we treated pericytes during early phases of reprogramming with recombinant *NODAL* (1  $\mu\text{g}/\text{mL}$ ) and *BMP4* (30  $\text{ng}/\text{mL}$ ; Fig. 4a,b). These treatments resulted in a significant reduction of reprogramming as determined by the number of *TUBB3*<sup>+</sup> cells amongst AS-transduced cells (Fig. 4c). Conversely, inhibition of *BMP*, *ACTIVIN/NODAL*, and *TGF- $\beta$*  signaling via the small molecules dorsomorphin (1  $\mu\text{M}$ ) and *SB431542* (10  $\mu\text{M}$ ) caused a threefold increase in the number of reprogrammed iNs (Fig. 4d,e). To address the relevance of *NOTCH* signaling in the reprogramming process, we treated AS-transduced pericytes with the  $\gamma$ -secretase inhibitor *N*-[*N*-(3,5-difluorophenacetyl)-*L*-alanyl]-*S*-phenylglycine *t*-butyl ester (*DAPT*). *DAPT* treatment (10  $\mu\text{M}$ ) resulted in a marked increase in the number of iNs (Fig. 4d,e). This finding is consistent with the role of *NOTCH* signaling in neurogenesis inhibition and neural stem cell maintenance<sup>23</sup>.

Though AS induction leads to productive iN reprogramming, we observed that maturation seemed to stall at 14 dpi, either because cells at later timepoints failed to mature further or because of a technical bias against harvesting healthy iNs at later stages (Fig. 3a). Our data showed that productive reprogramming involved inhibition of *BMP* signaling, and blocking *BMP* signaling appeared to promote maturation, as suggested by increased morphological iN complexity (Fig. 4e). We therefore analyzed the effect of the *BMP* inhibitor dorsomorphin during early phases of the reprogramming process on subsequent neuronal maturation (Fig. 5a). Dorsomorphin-treated AS-induced neurons exhibited markedly increased morphological complexity and soma size (Fig. 5b,c and Supplementary Fig. 4a), as well as increased membrane capacitance and decreased membrane resistance (Fig. 5d and Supplementary Fig. 4b). Single-cell RNA (scRNA)-seq on dorsomorphin-treated AS-induced neurons revealed that genes associated with synapse formation and synaptic function showed increased expression relative to untreated AS-transduced cells (Fig. 5e). In line with enhanced iN maturation, we also noted enhanced *GABA* and *PVALB* immunoreactivity (Supplementary Fig. 4c).

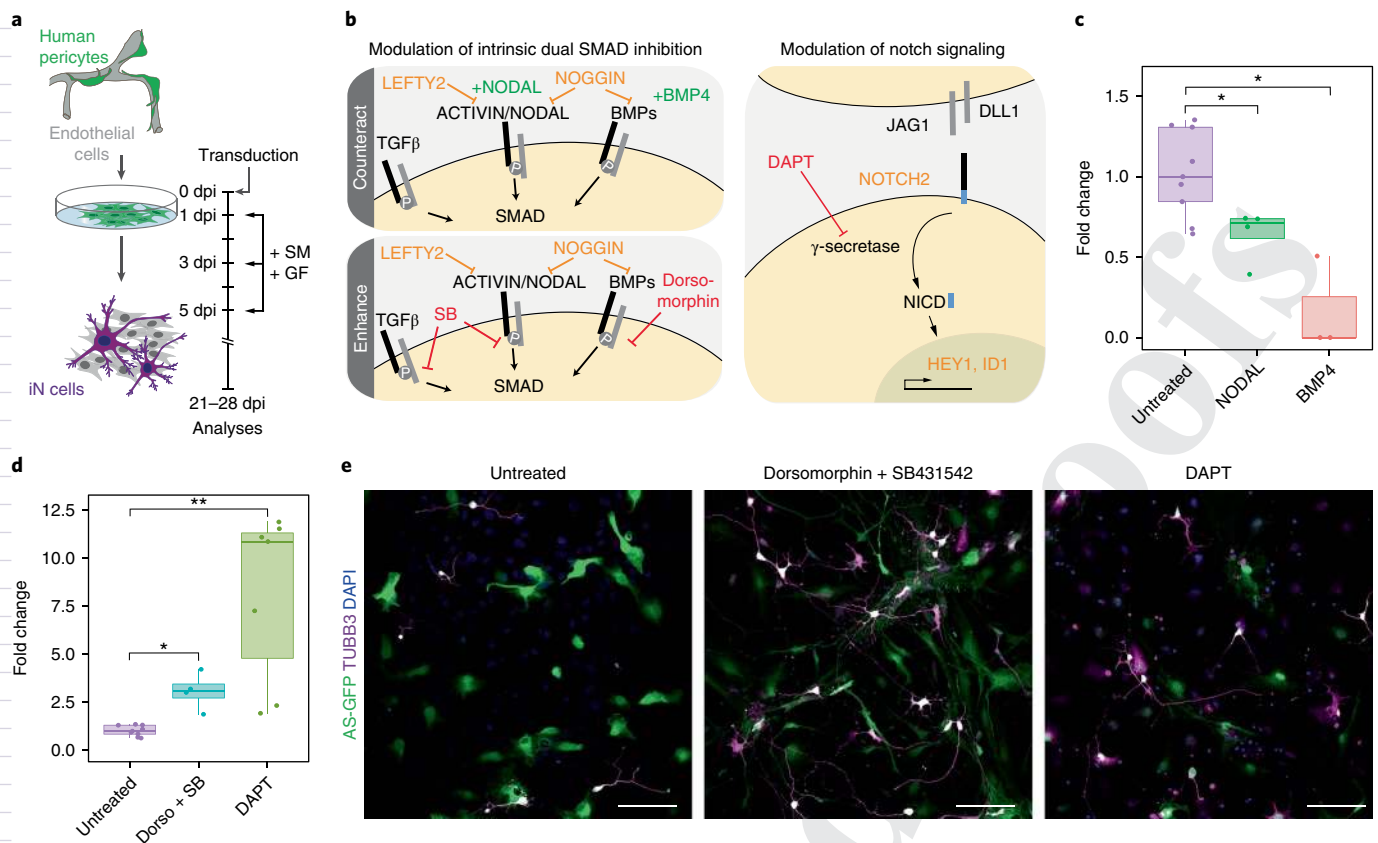


**Fig. 4 | Modulation of signaling pathways identified during neural stem cell-like state.** **a**, Schematic overview of the experimental timeline for the experiments contained in this figure. Cells were treated with either small molecules (SM) or growth factors (GF). **b**, Schematic overview of switch gene expression associated with signaling pathways and summary of treatments. **c**, Treatment with NODAL or BMP4 decreases the reprogramming efficiency. Reprogramming efficiency was calculated by quantifying TUBB3-immunoreactive cells among reporter-positive transduced cells 3–5 weeks after transduction with AS. Fold-changes were calculated by determining the ratio of growth factor in treated vs. nontreated TUBB3<sup>+</sup>Reporter<sup>+</sup> cells per total Reporter<sup>+</sup> cells of the transduced pericytes (dots represent independent individual experiments; untreated,  $n=9$ ; NODAL,  $n=4$ ; BMP,  $n=3$ ; data are represented as boxplots with whiskers; two-tailed unpaired Student's  $t$  test;  $P=0.01202$  for NODAL;  $P=0.01821$  for BMP4;  $*P<0.05$ ). Boxplots show median, quartiles (box), and range (whiskers). **d**, Reprogramming efficiencies (TUBB3<sup>+</sup>Reporter<sup>+</sup> cells per total Reporter<sup>+</sup> cells) increase following enhancing treatments with dorsomorphin (dorso) + SB431542 (SB) or DAPT. The fold change was calculated by determining the ratio of small-molecule-treated vs. nontreated TUBB3<sup>+</sup>Reporter<sup>+</sup> cells per total Reporter<sup>+</sup> cells of the transduced pericytes (dots represent independent individual experiments; untreated,  $n=9$ ; dorso + SB,  $n=4$ ; DAPT,  $n=7$ ; data are represented as boxplots with whiskers; two-tailed unpaired Student's  $t$  test;  $*P=0.02133$  for dorso + SB;  $**P=0.0050$  for DAPT). Boxplots show median, quartiles (box), and range (whiskers). **e**, Representative micrographs of AS-transduced pericyte cultures (green) and stained with anti-TUBB3 (magenta). Note the increased appearance of reprogrammed pericytes that acquired neuronal morphology following dorso + SB ( $n=4$ ) and DAPT ( $n=7$ ) treatment compared to the untreated cells. Nuclei are stained with DAPI. Scale bars, 50 μm.

**Bifurcation into distinct iN lineages.** These data prompted us to have a closer look at the neuronal subtype specification induced by AS with or without dorsomorphin (ASD). We focused on iNs that expressed both *SNAP25* and *MAP2* and analyzed 20 AS and 72 ASD cells. The majority of AS and ASD iNs exhibited a fore-brain GABAergic interneuron program characterized by coordinated expression of multiple members of the *DLX* gene family (Fig. 5f). Notably, we found evidence for further subspecification among the *DLX*-expressing iNs. We observed distinct clusters of *VIP*-expressing neurons, some of which also co-expressed *CCK*. Likewise, we noted two clusters specifically expressing *SST* (Fig. 5f).

However, we also noted a subset of iNs that expressed a transcription factor of the glutamatergic lineage, *NEUROG2*. Notably, these iNs also expressed downstream targets *NEUROD1* and *NEUROD4*, consistent with the expression of a telencephalic glutamatergic neuron program<sup>10,24</sup>. The fact that this subset also expressed *RELN* (Fig. 5f) may indicate that these iNs acquire a Cajal–Retzius neuron-like program. It is noteworthy that, while the majority of *DLX1*-expressing cells were *NEUROG2*<sup>-</sup> and many high-*NEUROG2*<sup>+</sup> cells

were *DLX1*<sup>-</sup>, we observed some outliers expressing both genes (Supplementary Fig. 4d). This may reflect the possibility that the definitive decision between the two major neuron lineages (*GABA* versus *glutamate*) had not yet taken place in these cells. To reveal the developmental trajectory toward a *DLX*- or *NEUROG2*-dominated fate, we employed pseudotemporal ordering of the transcriptomes of AS cells of the productive path and 14-dpi ASD cells. Notably, we observed a bifurcation of the trajectory into *DLX*- or *NEUROG2*-dominated pathways, which preceded neuronal differentiation marked by *SNAP25* expression (Fig. 5g and Supplementary Fig. 4e). Projecting the switch gene signature identified in Fig. 3c onto the reprogramming path revealed that the transient expression of neural stem cell-like genes occurred and ceased before lineage bifurcation (Fig. 5h). Consistent with the increased maturation of ASD cells, the distribution of ASD transcriptomes was shifted farther along the trajectory of pericyte-to-iN reprogramming (Fig. 5i). We corroborated the emergence of *DLX*- or *NEUROG2*-expressing inhibitory and excitatory neuronal lineages using an alternative scRNA-seq method and a second pericyte donor (Supplementary Fig. 5).



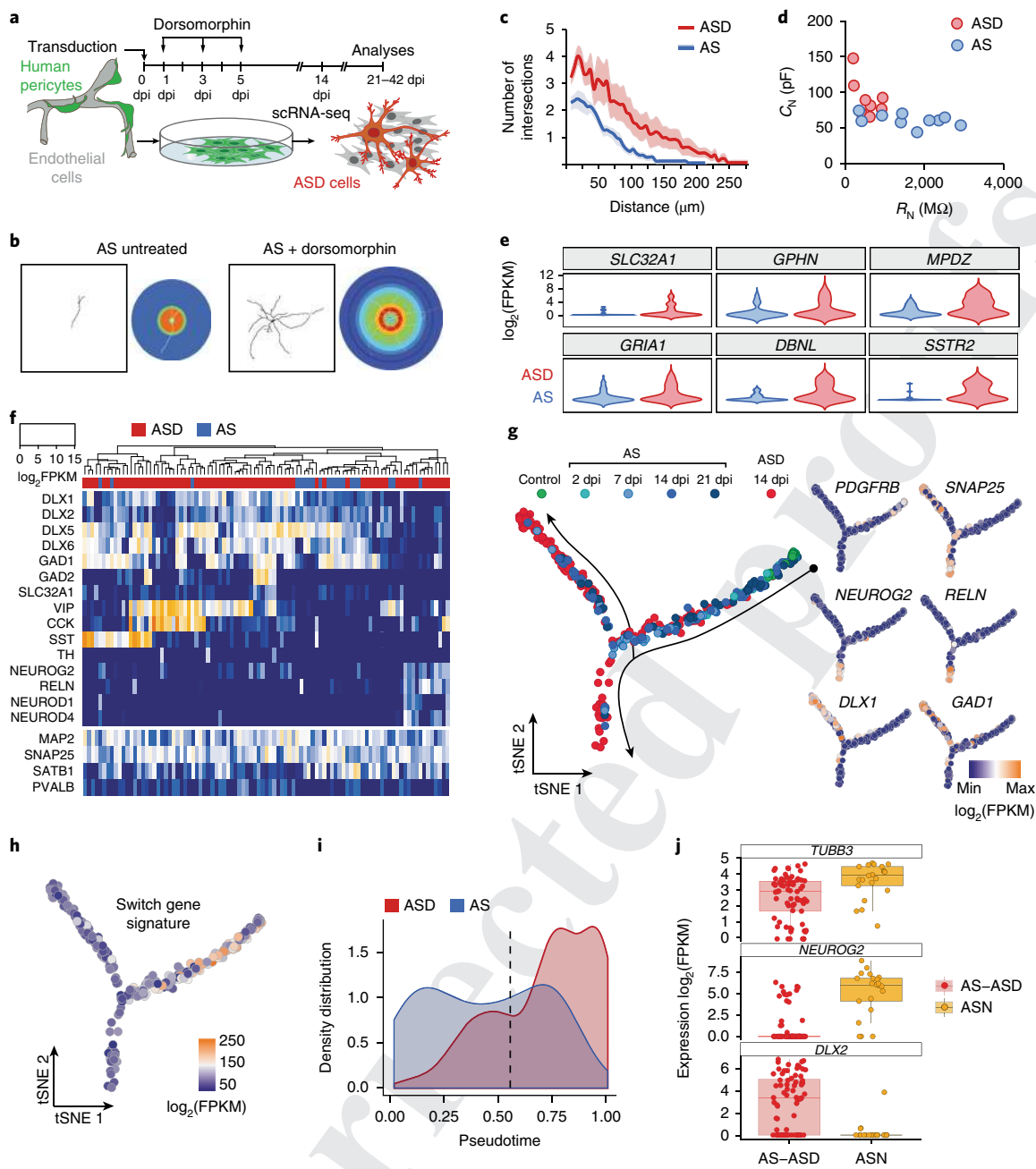


**Fig. 5 | Pericytes give rise to distinct neuronal subtypes, and targeting BMP signaling promotes maturation.** **a**, Schematic overview of experiments in this figure. **b**, Representative examples of untreated and dorsomorphin-treated AS-transduced pericytes showing complex branching of dendritic arbors in dorsomorphin-treated cells. Neuronal morphology was reconstructed using TUBB3 immunoreactivity and used for Sholl analyses. In the Sholl masks (right), warmer hues indicate higher number of intersections (untreated,  $n=14$  cells from 3 independent experiments; dorsomorphin-treated,  $n=14$  cells from 3 independent experiments). **c**, Single-cell neuromorphology reconstruction by Sholl analysis on dorsomorphin treated AS-transduced cells was compared to untreated cells. Note the increase in complexity of dorsomorphin-treated cells, which display more intersections with concentric shells and an overall increase in the length of the dendrites (see also Supplementary Fig. 4a). Data are represented in a line graph as mean  $\pm$  s.e.m. (shaded region) (untreated,  $n=14$  cells from 3 independent experiments; dorsomorphin-treated,  $n=14$  cells from 3 independent experiments). **d**, Electrophysiological assessment of AS and ASD cells. Membrane capacitance ( $C_N$ ) is plotted as a function of the membrane resistance ( $R_N$ ). AS cells have greater  $R_N$  but smaller  $C_N$  compared to ASD cells. **e**, Violin blots show the density distribution of expression of selected neuronal maturation genes in neuronal (SNAP25<sup>+</sup>, MAP2<sup>+</sup>, PDGFRB<sup>-</sup>) AS cells ( $n=20$ ) and ASD cells ( $n=75$ ). **f**, PCA followed by hierarchical clustering was used to characterize neuronal cells (SNAP25<sup>+</sup>, MAP2<sup>+</sup>, PDGFRB<sup>-</sup>) AS cells ( $n=20$ ) and ASD cells ( $n=75$ ) at 14 dpi according to their expression of neuronal genes. Note the different interneuron clusters marked by the expression of interneuron subtype-specific genes *VIP*, *SST*, and *CCK*. **g**, Monocle2 was used to compare maturation of AS and ASD cells. **h**, Switch gene signature from Fig. 3c projected onto pseudotemporal ordered transcriptomes from **g**. **i**, The density distributions (i.e., normalized cell numbers per timepoint of pseudotime) along the pseudotime of AS transcriptomes (14 dpi) from the productive path and ASD transcriptomes (from **g**) are plotted as a function of the distance from the start point. Note the shift of ASD cell transcriptomes compared to AS transcriptomes. The dotted line indicates the bifurcation point in **g**. **j**, Jitter-boxplot (boxplots show median, quartiles (box), and range (whiskers)) showing the expression of *TUBB3* in all SNAP25<sup>+</sup>, MAP2<sup>+</sup>, PDGFRB<sup>-</sup> AS and ASD ( $n=71$ ), and AS + overexpressed *NEUROG2* (ASN;  $n=21$ ) cells used for this analysis. Boxplots show the strong increase of *NEUROG2* and decrease in *DLX2* gene expression in ASN cells as compared to AS and ASD cells.



460 To test whether *NEUROG2* indeed suffices to induce a glutamatergic phenotype, we overexpressed *NEUROG2* alongside AS (Supplementary Fig. 4f). *NEUROG2* overexpression resulted in the almost complete suppression of *DLX2* (Fig. 5j), suggesting that *NEUROG2* can divert iNs from adopting predominantly a GABAergic phenotype toward generating mostly glutamatergic neurons. Accordingly, we found that *NEUROG2*-overexpressing AS neurons exhibited vesicular glutamate transporter immunoreactivity (Supplementary Fig. 4g).

## 470 Discussion

471 Here we have shown that reprogramming success of adult human brain pericytes into iNs by the transcription factors *Ascl1* and *Sox2* (AS) critically depends on cellular context, as revealed by the observation that pericyte heterogeneity is a key determinant for reprogramming competence. Successful reprogramming by AS encompasses the passage through a neural stem cell-like intermediate state, yet it occurs in the absence of cell division. Moreover, regulation of signaling pathways during the neural stem cell-like state was of functional importance for the reprogramming outcome. This data indicates that AS-mediated reprogramming involves the unfolding of developmental programs and argues for the engagement of hierarchical developmental gene-regulatory networks<sup>6</sup> rather than direct interconversion between two states of terminal differentiation. Finally, we found that, following the transition through a neural stem cell-like state, the reprogramming trajectory eventually bifurcates to give rise to two distinct branches characterized by *DLX*- or *NEUROG*-dominated gene expression and indicative of bifurcation into GABAergic or glutamatergic lineages, respectively. This provides a mechanistic explanation for the common observation that a single reprogramming cocktail can yield neurons of distinct neurotransmitter phenotypes<sup>15,25</sup>.

492 We observed that the reprogramming competence of adult human brain pericytes is highly variable and a main source for this variability is pericyte heterogeneity. Heterogeneity of pericytes has been described in many tissues and may reflect distinct embryonic origins<sup>26</sup>. Our scRNA-seq experiments revealed two distinct populations, one of which, characterized by high *LEPR* expression, displayed markedly reduced reprogramming propensity. Notably, a recent study using scRNA-seq showed that several of the heterogeneously expressed genes are also expressed at highly variable levels in acutely isolated human midbrain pericytes<sup>27</sup>, which might indicate that similar heterogeneity occurs in vivo. However, our study may actually underestimate overall pericyte heterogeneity, as we included in our scRNA-seq analysis only retrovirus-transduced cells, for which ongoing cell division at the time of transduction is required. We would also expect that proliferative pericytes do not perfectly match pericytes under resting conditions, but may be more akin to those found to undergo cell division in response to severe CNS injury<sup>28</sup>.

510 Revealing the cell-context requirements for reprogramming is of greatest importance if direct lineage reprogramming is to be of therapeutic value. Many reprogramming-factor cocktails that work well with mouse cells (for example, MEFs) are rather inefficient with human cells, and in particular, when the cells are of adult-tissue origin. It will be therefore a fruitful field of investigation to identify, in addition to transcriptome differences, epigenetic disparities between the two subpopulations of pericytes identified here. This may yield potential molecular targets for improved reprogramming strategies that may apply to other adult human somatic cell types.

520 A key finding of our study is the observation that AS-transduced cells pass through a neural stem cell-like state before differentiating into iNs. This neural stem cell-like state is characterized by expression of a battery of genes that are normally expressed in neural stem cells or progenitor cells during forebrain embryonic development, referred to here as switch genes as they are dynamically regulated

during the reprogramming process. While referring to the state characterized by switch gene expression as a neural stem cell-like state, we do not equate it to a bona fide neural stem cell state. This distinction is warranted given the absence of classical markers of neural stem cells such as *MSH1* (Musashi) or *NES* (Nestin) during the switch state, some anomalies in gene regulation such as *DLX5* expression preceding *DLX1* expression in time, and above all the absence of cell division and of a transcriptomic signature of an active cell cycle. We hypothesize that genes induced during the switch state represent a neural stem cell gene-expression module specifically regulated by *Ascl1* and *Sox2* and that other transcription factors may be required to induce other neural stem cell markers. Notably, the AS-induced neural stem cell expression module appears to be sufficient to drive the trajectory toward neuronal differentiation.

Switch genes include components of several signaling pathways, such as the *ACTIVIN/NODAL* (*LEFTY2*), *BMP* (*NOG*), and *NOTCH* (*HES5*, *HEY1*, *ID1*, *NOTCH2*) signaling pathways. By activating or inhibiting the *ACTIVIN/NODAL* and *BMP* pathways during the early phase of reprogramming through recombinant ligands or pharmacologically, we showed that these pathways exert an important influence on reprogramming efficiency. The fact that inhibition of *ACTIVIN/NODAL* and *BMP* signaling is required for reprogramming is consistent with the fact that inhibition of these pathways is important for neural induction during embryonic development<sup>22</sup>, can be used for driving human pluripotent stem cells toward neural lineages<sup>29</sup>, and enhances transcription factor-mediated reprogramming<sup>25,30</sup>. Crucially, we found that inhibition of *NOTCH* signaling promoted reprogramming. This is consistent with the role of *NOTCH* signaling in preventing neuronal differentiation of neural stem cells<sup>31</sup>. The conspicuous induction of the *NOTCH* ligand *DLL1* during reprogramming suggests that *DLL1*<sup>+</sup> cells exert a differentiation inhibitory effect on other AS-transduced cells, an inhibition that can be relieved pharmacologically. Notably, iNs appear to express *Myt1*, which has recently reported to be induced cell-autonomously by *Ascl1* and to repress *Notch* signaling<sup>32</sup>. Likewise, its close relative *Myt1l*, a widely used component of the *BAM* reprogramming cocktail, has been shown to repress *Notch* signaling<sup>12</sup>. This suggests that the *BAM* cocktail exhibits similarities to AS' mechanism of reprogramming, but that the addition of the postmitotic repressor *Myt1l* serves to curtail molecular pathways of the switch state that keep neuronal differentiation in check. Another intriguing aspect of *NOTCH2* expression during reprogramming is the fact that *Notch2* has been recently found to repress cell cycle-related genes and drive neural stem cells to quiescence, which may account in part for the lack of cell division during the switch state<sup>33</sup>.

Unexpectedly, we found that human brain pericytes reprogrammed by AS bifurcate into lineages dominated by transcription factors that specify inhibitory and excitatory neuron fates. This bifurcation was corroborated using two distinct scRNA-seq platforms (Fluidigm C1 and 10×Genomics). While the *DLX* gene family-dominated branch was enriched for genes characteristic of GABAergic neuron lineage (for example, *GAD1* and *GAD2*), the *NEUROG*-expressing branch expressed other transcription factors characteristic of the glutamatergic neuron lineage, such as *NEUROD1* and *NEUROD4*. Moreover, cells of the latter lineage also expressed *RELN*, suggesting similarities to the Cajal-Retzius subtype of glutamatergic neurons. The fact that forced expression of *Neurog2* in AS-transduced pericytes suppresses *DLX* gene expression may indicate that lineage bifurcation is driven by mutual cross-repression of *NEUROG* and *DLX* family genes. Our data raise the intriguing possibility that the bipotent neural stem cell-like state observed during AS reprogramming relates to the suggested common precursor generating both glutamatergic and GABAergic neurons in the cerebral cortexes of human and nonhuman primates<sup>34</sup>.

Overall, our study not only provides new insights into the biology underlying iN reprogramming, but also sheds light on the capacity of two transcription factors, *Ascl1* and *Sox2*, to cooperate in the generation of diverse neuronal subtypes, a cooperation that may be relevant during human brain development. The identification of molecular programs that establish cellular intermediates and lineage bifurcations during iN reprogramming provides avenues for improving lineage conversion of human brain-resident cells toward therapeutically relevant cell types.

## Methods

Methods, including statements of data availability and any associated accession codes and references, are available at <https://doi.org/10.1038/s41593-018-0168-3>.

Received: 12 February 2018; Accepted: 17 April 2018;

## References

- Heinrich, C., Spagnoli, F. M. & Berninger, B. In vivo reprogramming for tissue repair. *Nat. Cell Biol.* **17**, 204–211 (2015).
- Amamoto, R. & Arlotta, P. Development-inspired reprogramming of the mammalian central nervous system. *Science* **343**, 1239882 (2014).
- Mertens, J., Marchetto, M. C., Bardy, C. & Gage, F. H. Evaluating cell reprogramming, differentiation and conversion technologies in neuroscience. *Nat. Rev. Neurosci.* **17**, 424–437 (2016).
- Srivastava, D. & DeWitt, N. In vivo cellular reprogramming: the next generation. *Cell* **166**, 1386–1396 (2016).
- Ruiz, S. et al. A high proliferation rate is required for cell reprogramming and maintenance of human embryonic stem cell identity. *Curr. Biol.* **21**, 45–52 (2011).
- Morris, S. A. Direct lineage reprogramming via pioneer factors; a detour through developmental gene regulatory networks. *Development* **143**, 2696–2705 (2016).
- Vierbuchen, T. & Wernig, M. Molecular roadblocks for cellular reprogramming. *Mol. Cell* **47**, 827–838 (2012).
- Gascón, S., Masserdotti, G., Russo, G. L. & Götz, M. Direct neuronal reprogramming: achievements, hurdles, and new roads to success. *Cell Stem Cell* **21**, 18–34 (2017).
- Wapinski, O. L. et al. Hierarchical mechanisms for direct reprogramming of fibroblasts to neurons. *Cell* **155**, 621–635 (2013).
- Masserdotti, G. et al. Transcriptional mechanisms of proneural factors and REST in regulating neuronal reprogramming of astrocytes. *Cell Stem Cell* **17**, 74–88 (2015).
- Treutlein, B. et al. Dissecting direct reprogramming from fibroblast to neuron using single-cell RNA-seq. *Nature* **534**, 391–395 (2016).
- Mall, M. et al. Myt1l safeguards neuronal identity by actively repressing many non-neuronal fates. *Nature* **544**, 245–249 (2017).
- Heinrich, C. et al. Directing astroglia from the cerebral cortex into subtype specific functional neurons. *PLoS Biol.* **8**, e1000373 (2010).
- Chanda, S., Marro, S., Wernig, M. & Südhof, T. C. Neurons generated by direct conversion of fibroblasts reproduce synaptic phenotype caused by autism-associated neuroligin-3 mutation. *Proc. Natl Acad. Sci. USA* **110**, 16622–16627 (2013).
- Vierbuchen, T. et al. Direct conversion of fibroblasts to functional neurons by defined factors. *Nature* **463**, 1035–1041 (2010).
- Karow, M. et al. Reprogramming of pericyte-derived cells of the adult human brain into induced neuronal cells. *Cell Stem Cell* **11**, 471–476 (2012).
- Long, J. E. et al. *Dlx1&2* and *Mash1* transcription factors control striatal patterning and differentiation through parallel and overlapping pathways. *J. Comp. Neurol.* **512**, 556–572 (2009).
- Liu, S. J. et al. Single-cell analysis of long non-coding RNAs in the developing human neocortex. *Genome Biol.* **17**, 67 (2016).
- Raposo, A.A. et al. *Ascl1* coordinately regulates gene expression and the chromatin landscape during neurogenesis. *Cell Rep.* <https://doi.org/10.1016/j.celrep.2015.02.025> (2015).
- Trapnell, C. et al. The dynamics and regulators of cell fate decisions are revealed by pseudotemporal ordering of single cells. *Nat. Biotechnol.* **32**, 381–386 (2014).
- Camp, J. G. et al. Human cerebral organoids recapitulate gene expression programs of fetal neocortex development. *Proc. Natl Acad. Sci. USA* **112**, 15672–15677 (2015).
- Suzuki, I. K. & Vanderhaeghen, P. Is this a brain which I see before me? Modeling human neural development with pluripotent stem cells. *Development* **142**, 3138–3150 (2015).
- Imayoshi, I., Sakamoto, M., Yamaguchi, M., Mori, K. & Kageyama, R. Essential roles of Notch signaling in maintenance of neural stem cells in developing and adult brains. *J. Neurosci.* **30**, 3489–3498 (2010).
- Guillemot, F. Spatial and temporal specification of neural fates by transcription factor codes. *Development* **134**, 3771–3780 (2007).
- Ladewig, J. et al. Small molecules enable highly efficient neuronal conversion of human fibroblasts. *Nat. Methods* **9**, 575–578 (2012).
- Dias Moura Prazeres, P. H. et al. Pericytes are heterogeneous in their origin within the same tissue. *Dev. Biol.* **427**, 6–11 (2017).
- La Manno, G. et al. Molecular diversity of midbrain development in mouse, human, and stem cells. *Cell* **167**, 566–580.e19 (2016).
- Göriz, C. et al. A pericyte origin of spinal cord scar tissue. *Science* **333**, 238–242 (2011).
- Chambers, S. M. et al. Highly efficient neural conversion of human ES and iPS cells by dual inhibition of SMAD signaling. *Nat. Biotechnol.* **27**, 275–280 (2009).
- Liu, M. L. et al. Small molecules enable neurogenin 2 to efficiently convert human fibroblasts into cholinergic neurons. *Nat. Commun.* **4**, 2183 (2013).
- Kageyama, R., Ohtsuka, T., Shimojo, H. & Imayoshi, I. Dynamic regulation of Notch signaling in neural progenitor cells. *Curr. Opin. Cell Biol.* **21**, 733–740 (2009).
- Vasconcelos, F. F. et al. MyT1 counteracts the neural progenitor program to promote vertebrate neurogenesis. *Cell Rep.* **17**, 469–483 (2016).
- Engler, A. et al. Notch2 signaling maintains NSC quiescence in the murine ventricular-subventricular zone. *Cell Rep.* **22**, 992–1002 (2018).
- Radonjić, N. V. et al. Diversity of cortical interneurons in primates: the role of the dorsal proliferative niche. *Cell Rep.* **9**, 2139–2151 (2014).

## Acknowledgements

We thank M. Wernig (Stanford University) for generously providing us with the *Sox2* coding sequence. We are also very grateful to B. Sutor (BMC, LMU Munich) for help with the electrophysiological experiments, R. Menon (UMC Mainz) for help with the cell culture experiments, A. Bosio (Miltenyi Biotec) for help with the multidimensional fluorescence stainings, and F. Calzolari (UMC Mainz) for comments on the manuscript. We thank B. Höber, A. Weihmann, and J. Kelso of MPI-EVA for sequencing and bioinformatics support with this project. Flow cytometric cell sorting was performed at the “Core Unit Durchflusszytometrie” (CUDZ) of the Center for Infectious Diseases at the College of Veterinary Medicine, University of Leipzig, Leipzig, Germany. S.F. was supported by a fellowship from the Swiss National Science Foundation (PA00P3\_139709). W.F. was supported by a Fellowship from the China Research Council. This work was supported by the following grants: advanced ERC ChroNeuroRepair to M.G.; Bavarian State Ministry of Sciences, Research and the Arts to M.K. and B.B. (ForiPS D2-F2412.26); Schram foundation (T287/29577/2017) and Wings For Life (WFL-DE-012/14) to M.K.; Max Planck Society to B.T.; and DFG (INST 161/875-2; BE 4182/8-1), NEURON ERA-NET (01EW1604), and Wellcome Trust (206410/Z/17/Z) to B.B.

## Author contributions

M.K., J.G.C., B.T., and B.B. conceived the study and designed experiments; M.K. performed direct reprogramming experiments; M.K., S.F., A.P., and V.K.T. analyzed bulk RNA-seq data; A.B. helped with processing of the 10xGenomics data; A.G. performed RNA isolation for bulk RNA-seq analysis; W.F. performed time-lapse imaging experiments; T.R. performed electrophysiological recordings; A.C. performed Sholl analyses; A.S. performed immunocytochemical analyses; C.S. provided human brain biopsies; M.G. provided material; J.G.C., M.G.-S., and T.G. performed single-cell RNA-seq experiments and sequenced libraries; J.G.C., J.K., and B.T. analyzed single-cell RNA-seq data; all authors discussed the data; and M.K., J.G.C., S.F., B.T., and B.B. wrote the paper.

## Competing interests

The authors declare no competing interests.

## Additional information

Supplementary information is available for this paper at <https://doi.org/10.1038/s41593-018-0168-3>.

Reprints and permissions information is available at [www.nature.com/reprints](http://www.nature.com/reprints).

Correspondence and requests for materials should be addressed to M.K. or B.T. or B.B.

**Publisher's note:** Springer Nature remains neutral with regard to jurisdictional claims in published maps and institutional affiliations.



## 592 Methods

593 **Culture of primary human pericytes.** Primary pericytes were derived as  
594 described previously from adult human brain tissue<sup>16,35</sup>. Briefly, specimens of  
595 cerebral cortex were obtained from standard surgical interventions of patients  
596 aged 19–70 years old and of both sexes. The study was approved by the ethical  
597 committee of the Medical Faculty of the LMU Munich, and written informed  
598 consent was obtained from all patients. Human tissue was enzymatically (TrypLE,  
599 Life technologies) and mechanically dissociated, and, following centrifugation at  
600 1,000 rpm for 5 min and resuspension in pericyte medium, cells were plated in  
601 T75 cell-culture flasks. Pericyte growth medium consisted of DMEM high glucose  
602 with Glutamax, 20% FBS, and penicillin/streptomycin. Medium was changed  
603 twice per week and subcultivation at a ratio of 1:3 was performed every 10–14 d.  
604 Cells were grown under low-oxygen conditions (5% O<sub>2</sub>, 5% CO<sub>2</sub>; Galaxy 170R,  
605 New Brunswick).

606 **Retroviral transduction and treatments of human pericytes.** The retroviral  
607 backbone used for lineage conversion of pericytes into iNs allowed for the  
608 polycistronic expression of *Ascl1* and *Sox2* (connected via p2A) under the control  
609 of an internal chicken  $\beta$ -actin promoter with cytomegalovirus enhancer (CAG)  
610 together with either *DsRed* or *GFP* downstream of an internal ribosomal entry site  
611 (IRES). For control, cultures were transduced with a virus encoding only *DsRed* or  
612 *GFP* behind an IRES site as described previously<sup>13,16</sup>.

613 Retroviral transduction of primary pericyte cultures was performed 24 h after  
614 plating on either poly-D-lysine-coated glass coverslips or in T25 or T75 cell-culture  
615 flasks without coating, using VSV-G (vesicular stomatitis virus glycoprotein)-  
616 pseudotyped retroviruses encoding neurogenic fate determinants as described  
617 previously<sup>16,35</sup>. Samples (pericyte donors, coverslips in 24-well plates or in T25 or  
618 T75 cell-culture flasks) were randomly assigned for transduction with different  
619 viruses. Twenty-four hours after transduction, the medium was replaced by a  
620 differentiation medium consisting of DMEM high glucose with Glutamax and B27  
621 supplement (Gibco). For growth factor or small-molecule treatments, addition  
622 was performed 1, 3, and 5 d following transduction. Factors were added to a final  
623 concentration of 1  $\mu$ M<sup>30,36</sup> for dorsomorphin (Sigma-Aldrich), 10  $\mu$ M for DAPT  
624 [*N*-[*N*-(3,5-difluorophenacetyl)-L-alanyl]-*S*-phenylglycine *t*-butyl ester; Stem Cell  
625 Technologies], 10  $\mu$ M<sup>37,38</sup> for SB431542 (Stem Cell Technologies), 30 ng/mL<sup>39,40</sup>  
626 for recombinant human BMP4 (Preprotech), and 1  $\mu$ g/mL<sup>41,42</sup> for recombinant  
627 human NODAL (RnD Systems). Cells were allowed to differentiate under low-  
628 oxygen conditions (5% O<sub>2</sub>, 5% CO<sub>2</sub>). Reprogramming efficiency was calculated  
629 by quantifying TUBB3-immunoreactive cells among reporter-positive transduced  
630 cells 3–5 weeks following transduction with retroviruses.

631 **Fluorescence-activated cell sorting (FACS).** For sorting of transduced cells  
632 for further culturing, bulk RNA-sequencing, or scRNA-sequencing, primary  
633 pericytes were detached from the culture dish using TrypLE for 4–6 min and  
634 subsequently resuspended in 500–1,000  $\mu$ L pericyte growth medium. Cell sorting  
635 was performed by taking advantage of the combined expression of *Ascl1* and *Sox2*  
636 with a fluorescent reporter protein (either *DsRed* or *GFP*). Gating was achieved  
637 via subtracting the autofluorescence of nontransduced cells; control (*DsRed* or  
638 *GFP* only)-transduced cells were used as respective controls. Following sorting,  
639 cells were (i) collected in pericyte growth medium and plated on PDL-coated glass  
640 cover slips on 24-well plates for further culturing, (ii) directly collected into RLT  
641 buffer (Qiagen) and stored at –80 °C until RNA isolation for bulk RNA-seq, or  
642 (iii) prepared for single-cell loading onto a C1 Fluidigm chip for scRNA-seq. To  
643 separate LEPR<sup>+</sup> and LEPR<sup>-</sup> pericyte populations, pericyte cultures were detached  
644 from the culture dish using TrypLE for 4–6 min and subsequently 1  $\times$  10<sup>5</sup>–5  $\times$  10<sup>5</sup>  
645 cells were resuspended in 100  $\mu$ L staining solution (PBS plus 0.5% BSA). Primary  
646 antibody (Alexa Fluor 647-conjugated CD295 (anti-LEPR; 1:20, BD Pharmingen,  
647 cat.no. 564376) was added and cells were incubated for 30 min on ice in the dark.  
648 After washing three times in staining solution, cells were resuspended in 500  $\mu$ L  
649 pericyte growth medium and subjected to cell sorting using a FACS Aria (BD). An  
650 Alexa Fluor 647-conjugated isotype control antibody (1:100, BD Pharmingen) was  
651 used to gate the proper populations.

652 **Immunohistochemical staining.** Cell cultures were fixed in 4% paraformaldehyde  
653 (PFA) in phosphate-buffered saline (PBS) for 15 min at room temperature. Cells  
654 were first pretreated in blocking solution consisting of 0.2–0.5% Triton X-100 and  
655 10% donkey serum in PBS for 60 min, followed by incubation with the primary  
656 antibodies in 100  $\mu$ L in the same solution for 1 h at room temperature or overnight  
657 at 4 °C. After extensive washing in PBS, cells were incubated in the same solution  
658 with appropriate species- or subclass-specific secondary antibodies conjugated  
659 to fluorophores. Coverslips were finally mounted onto a glass slide with an anti-  
660 fade mounting medium (Aqua Poly/Mount; Polysciences, Warrington, PA). For  
661 multidimensional immunofluorescence staining, fixed cell cultures were subjected  
662 to sequential immunofluorescence staining/destaining cycles adapted from a  
663 technique published by Schubert et al.<sup>43</sup>.

664 **Microscopy and time-lapse imaging.** Immunocytochemical stainings were  
665 first examined with an epifluorescence microscope (BX61, Olympus) equipped  
666 with the appropriate filter sets. Stainings were further analyzed with a LSM710

667 laser-scanning confocal microscope (Carl Zeiss.). Digital images were captured  
668 using the ZEN software (Carl Zeiss).

669 We performed time-lapse microscopy to follow the reprogramming process  
670 of pericytes into iNs. Pericytes were transduced with *Ascl1*-*Sox2*-CAG-GFP  
671 retrovirus. Twenty-four hours after transduction, medium was replaced by a  
672 differentiation medium consisting of DMEM high glucose with Glutamax and  
673 B27 supplement (Gibco). The microwell plate containing these cells was 48 h  
674 later placed on a heated microscopic stage with 5% CO<sub>2</sub> and 37 °C and imaged  
675 continuously for up to 14 dys. Fluorescent images were taken subsequently once  
676 every 4 h and brightfield images once every 5 min. After completion of time-lapse  
677 imaging, cells were fixed with 4% PFA, and after imaging ICC was performed  
678 to corroborate the results from the imaging. Data analysis was performed using  
679 Timm's Tracking Tool (TTT) software.

680 **Sholl analysis.** Sholl analysis was performed by using the ImageJ plugin Sholl  
681 Analysis<sup>44</sup>. Confocal images of iNs with immunocytochemical stainings against  
682 TUBB3 were used for tracing individual neuronal processes of selected cells in  
683 ImageJ (Fiji) software<sup>45</sup>. After assigning the center of each cell soma, a grid with  
684 concentric circles with increasing diameter (5  $\mu$ m) was superimposed. The data  
685 are expressed as the mean  $\pm$  s.e.m. of the values obtained in four independent  
686 experiments; untreated  $n = 14$ , dorsomorphin-treated  $n = 14$ . The investigators  
687 carried out blinded analyses.

688 **Neuromorphometry.** Several parameters of cell morphology were examined.  
689 Neuronal complexity quantification was conducted with the following  
690 measurements: (i) primary branches, i.e., processes emerging directly from the  
691 soma per neuron; (ii) dendritic segment, i.e., part of the dendrite between two  
692 branching points; (iii) branching point, i.e., the point at the dendrite where a  
693 dendrite ramifies into two or more; (iv) maximum dendritic length or ending  
694 radius, i.e., the radius of the largest circle of the superimposed Sholl mask; (v)  
695 soma size (in  $\mu$ m<sup>2</sup>), i.e., cross sectional surface area of the cell body; and (vi) sum  
696 of intersections, i.e., the sum of all intersections between the dendritic arbors  
697 and the concentric circles radiating from the cell body. The numbers of primary  
698 branches, as well as the numbers of dendritic segments and branching points, were  
699 counted manually. ImageJ Fiji software was used to measure soma size. The sum  
700 of intersections and the ending radius were measured using the Sholl method (see  
701 “Sholl analysis” section, above).

702 **Statistics.** To test for statistical significance, two-tailed unpaired Student's *t* tests  
703 were used. Asterisks indicate statistically significant differences across the two  
704 groups: \* $P < 0.05$ , \*\* $P < 0.01$ , \*\*\* $P < 0.001$ . The analyses were done using Prism  
705 (GraphPad) or R. Data distribution was assumed to be normal, but this was not  
706 formally tested. Throughout the study, boxplots show medians, quartiles (box), and  
707 ranges (whiskers). No statistical methods were used to predetermine sample sizes,  
708 but our sample sizes are similar to those reported in previous publications<sup>11,16</sup>. If  
709 not indicated otherwise, data collection and analysis were not performed blind to  
710 the conditions of the experiments. No data points were excluded from the analysis,  
711 except for cells in the scRNA-seq analyses that did not fulfill the required criteria  
712 (see below sections on scRNA-seq analyses).

713 **Electrophysiology.** For electrophysiological recordings, coverslips with  
714 reprogrammed cells were transferred to a recording chamber mounted on the stage  
715 of an upright microscope (Axioscope FS, Zeiss, Germany). Cells were perfused  
716 with a bathing solution consisting of (in mM): NaCl 150, KCl 3, CaCl<sub>2</sub> 3, MgCl<sub>2</sub> 2,  
717 HEPES 10, and D-glucose 10. The pH of the solution was adjusted to 7.4 (NaOH);  
718 the osmolarity ranged from 309 to 313 mOsmol. All recordings were performed at  
719 room temperature (23–24 °C). Electrodes for whole-cell patch-clamp recordings  
720 were fabricated from borosilicate glass capillaries (OD: 1.5 mm, ID: 0.86 mm; Hugo  
721 Sachs Elektronik-Harvard Apparatus) and filled with a solution composed of (in  
722 mM): potassium-gluconate 135, KCl 4, NaCl 2, EGTA 0.2, HEPES (potassium salt)  
723 10, adenosine-triphosphate (magnesium salt, ATP[Mg]) 4, sodium guanosine-  
724 triphosphate (NaGTP) 0.5, and phosphocreatine 10 (pH: 7.25–7.30, osmolarity:  
725 288–291 mOsmol). The electrodes (resistance: 5–7 M $\Omega$ ) were connected to the  
726 headstage of a NPI ELC-03XS amplifier (NPI, Tamm, Germany). To visualize the  
727 cultured cells, the microscope was equipped with differential interference contrast  
728 (DIC) optics and with epifluorescence optics for green and red fluorescence  
729 (filter sets: Sachs BP450–490, LP520, Zeiss BP546/12, LP590). Images were taken  
730 and displayed using a software-operated CCD microscope camera (ORCA R,  
731 Hamamatsu, Germany). Following membrane rupture, the cells were voltage-  
732 clamped to a holding potential of –60 mV and kept under this condition until  
733 the holding current stabilized (3–5 min). Then the amplifier was switched to  
734 current-clamp mode. The recorded signals were amplified ( $\times 10$ ), filtered at 10 or  
735 20 kHz (current clamp) and at 5 kHz (voltage clamp), digitized at a sampling rate  
736 of 10 or 20 kHz and stored on a computer for offline analysis. Data acquisition  
737 and generation of command pulses was done using a CED 1401 Micro 3 system in  
738 conjunction with Signal6 data acquisition software (Cambridge electronic design).  
739 Data analysis was performed using Igor Pro 6 (WaveMetrics, Lake Oswego,  
740 USA) together with the NeuroMatic IGOR plugin ([www.neuromatic.thinkrandom.com](http://www.neuromatic.thinkrandom.com)).  
741 Determination of the input resistance, RN, was performed by measuring the



658 amplitude of a voltage deviation induced by a small hyperpolarizing current  
659 pulse (1 s, 2–10 pA). The total membrane capacity CN was estimated  
660 using a method described by Zemankovics et al.<sup>46</sup>. The ability of the cells to  
661 generate action potentials was tested by injecting depolarizing current pulses  
662 (50 ms) with increasing current strengths ( $\Delta I$ : 2–10 pA) or by depolarizing  
663 current ramps (50 ms) from 0–100 pA. Spike discharge was analyzed by injecting a  
664 series of depolarizing current pulses (duration: 1 s) with a stepwise increment  
665 ( $\Delta I$ : 2–10 pA).

665 **Bulk RNA sequencing.** Primary pericytes from three different human donors were  
666 transduced with Ascl1, Sox2, AS, and/or control retroviruses and purified by FACS  
667 at 2 and 7 dpi. RNA was isolated using the RNeasy Micro Kit (Qiagen). Following  
668 Ribo-Zero removal, the RNA-seq library was prepared in accordance with  
669 Illumina's instructions using oligo-dT primers. The RNA-seq output in FASTQ  
670 format was aligned to the human hg38 genome (sourced from UCSC) using  
671 TopHat v2.0.8<sup>47</sup> and only uniquely mapped reads were retained for further analysis.  
672 SAMTOOLS v.0.1.19<sup>48</sup> was used for file format conversions (SAM and BAM). The  
673 read counts per gene were calculated using HTSeq v0.5.4p1<sup>49</sup>. The DESeq package<sup>50</sup>  
674 was used thereafter for differential expression analysis.  $P_{adj}$  values were calculated  
675 with the Benjamini–Hochberg procedure.

675 **GO terms analysis of bulk RNA-seq data.** GO enrichment analysis was performed  
676 using the Bioconductor package TopGO employing the default algorithm weight01<sup>51</sup>.  
677 Genes were considered significantly deregulated with  $P_{adj} < 0.01$ . GO terms were  
678 ordered according to their significance as determined by Fisher's exact test.

679 **Capture of single cells and preparation of cDNA.** Transduced human brain  
680 pericytes were sorted using FACS and single cells were captured on a medium-  
681 sized (10- to 17- $\mu$ m cell diameter) microfluidic RNA-seq chip using the Fluidigm  
682 C1 system. Cells were loaded onto the chip at a concentration of 350–500 cells per  
683  $\mu$ L and imaged by phase-contrast to assess number of cells per capture site. Only  
684 single cells were included in the analysis. cDNAs were prepared on chip using the  
685 SMARTer v4 Ultra Input Low RNA kit for Illumina (Clontech).

686 **RNA-seq library construction and cDNA sequencing.** Size distribution and  
687 concentration of single-cell cDNA was assessed on a capillary electrophoresis-  
688 based fragment analyzer (Advanced Analytical Technologies), and only single  
689 cells with high quality cDNA were further processed. Sequencing libraries  
690 were constructed in 96-well plates using the Illumina Nextera XT DNA Sample  
691 Preparation kit, using primer sets A and B according to the protocol supplied  
692 by Fluidigm and as described previously<sup>41</sup>. Libraries were quantified by Agilent  
693 Bioanalyzer using a High Sensitivity DNA analysis kit, as well as fluorimetrically  
694 using Qubit dsDNA HS Assay kits and a Qubit 2.0 Fluorimeter (Invitrogen,  
695 Thermo Fisher Scientific). Up to 192 single-cell libraries were pooled and 100-bp  
696 paired-end sequenced on one lane of the Illumina HiSeq 2500 to a depth of at  
697 least 500,000 reads per cell. Base calling, adaptor trimming, and de-multiplexing  
698 was performed as described<sup>52,53</sup>. The transcriptomes of a total of 769 cells was  
699 measured from the following 12 independent experiments: 2-dpi control (76 cells,  
700 1 experiment), 2-dpi Ascl1-only (82 cells, 1 experiment), 7-dpi Ascl1-only (64 cells,  
701 1 experiment), 2-dpi AS (86 cells, 1 experiment), 7-dpi AS (48 cells, 1 experiment),  
702 14-dpi AS (79 cells, 2 experiments), 21/22-dpi AS (130 cells, 2 experiments), 14-  
703 dpi ASD (183 cells, 2 experiments), and 14-dpi ASN (21 cells, 1 experiment). See  
704 Supplementary Table 5 for the transcriptome data for all 769 cells with annotations  
705 (quantification in log<sub>2</sub>(FPKM)).

706 **Processing, analysis, and graphic display of single-cell RNA-seq data.** Reads  
707 were aligned to a Bowtie2<sup>54</sup>-indexed human genome (hg38 sourced from Ensembl)  
708 supplemented with DNA sequences for *Egfp*, *mCherry*, *DsRed*, mouse *Ascl1*, and  
709 mouse *Sox2* using TopHat<sup>47</sup> with default settings. Transcript levels were quantified  
710 as fragments per kilobase of mapped reads (FPKM) generated by Cufflinks<sup>55</sup>  
711 using GENCODE protein-coding genes (hg38 Havana). We excluded cells that  
712 had less than 100,000 reads, expressed  $< 1,000$  genes, or did not express either of  
713 two housekeeping genes *ACTB* and *GAPDH*. Transcript levels were converted  
714 to the log<sub>2</sub>-space by taking the log<sub>2</sub>(FPKM). R studio (<https://www.rstudio.com/>)  
715 was used to run custom R scripts to perform PCA (FactoMineR package) and  
716 hierarchical clustering (stats package) and to construct heatmaps, correlation plots,  
717 scatter plots, violin plots, dendrograms, bar graphs, and histograms. Generally,  
718 ggplot2 and gplots packages were used to generate data graphs. The Seurat package  
719 implemented in R was used to identify cell clusters and perform differential gene  
720 expression based on t-SNE<sup>56</sup>. The Monocle2 package<sup>50</sup> was used to analyze cell  
721 lineage relationships. Covariance network analysis and visualizations were done  
722 using igraph implemented in R (<http://igraph.org/>). Signatures were calculated  
723 by summing the log<sub>2</sub>(FPKM) expression values of each gene in a set of genes  
724 comprising a signature (Supplementary Table 6).

725 **10× Genomics scRNA-seq experiment.** For the 10× Genomics experiment, cells  
726 were transfected with AS, treated with dorsomorphin, and analyzed at 14 dpi.  
727 Cells were sorted based on the expression of GFP and used for one encapsulation.  
728 10× Genomics sample libraries were sequenced on an Illumina HiSeq 2500 and

base calling, adaptor trimming, and de-multiplexing of single cells were performed  
using 10× Genomics Cell Ranger 2.0 software. We performed PCA and t-SNE  
analyses using the Seurat v2.0 package for R on 3,419 single cells with 1,000–  
7,000 genes detected (Supplementary Table 7). We used genes correlating and  
anticorrelating with the first eight principal components to cluster the cells, and  
found that clustering patterns were robust across multiple PC inclusions. Neuronal  
cluster-specific markers were found using Seurat's implementation of the 'bimod'  
likelihood-ratio test for single-cell gene expression data, and the top genes were  
selected based on the average log fold-change.

**Antibodies.** The following antibodies were used: mouse (IgG2b) anti-TUBB3  
(Sigma; cat. no. T8660; 1:300), rat IgG2a anti-CD49f-PE (Miltenyi Biotec; cat. no.  
130-100-096; 1:11), recombinant human anti-CD4 (Miltenyi; cat. no. 130-109-  
537; 1:11), rabbit anti-GABA (Abcam; cat. no. ab17413; 1:1,000), chick anti-GFP  
(Aves; cat. no. GFP-1020; 1:500), mouse (IgG1) anti-Pvalb (Swant; cat. no. PV-235;  
1:1,000), rabbit anti-Pdgfrb (Cell Signaling; cat. no. 3169S; 1:300), rat anti-RFP  
(Chromotek; cat. no. 5F8; 1:500), mouse (IgG2b) anti-SMA (Sigma; cat. no. A5228;  
1:500), and rabbit anti-VGLUT1 (Synaptic Systems, cat. no. 135302; 1:500). For  
FACS we additionally used mouse (IgG2b) anti-LEPR Al647 (BD Pharmingen;  
cat. no. 564376; 1:20) and corresponding isotype control (BD Pharmingen; cat.  
no. 557903; 1:20). Antibodies were selected according to the antibody validation  
reported by the distributing companies.

**Accession codes.** GEO: scRNA-seq data, [GSE113036](https://www.ncbi.nlm.nih.gov/geo/query/acc.cgi?acc=GSE113036).

**Reporting Summary.** Further information on experimental design is available in  
the Nature Research Reporting Summary linked to this article.

**Data availability and accession codes.** The scRNA-seq data used in this study  
have been deposited in the Gene Expression Omnibus (GEO) under accession  
number [GSE113036](https://www.ncbi.nlm.nih.gov/geo/query/acc.cgi?acc=GSE113036). The data that support the findings of this study are available  
from the corresponding author upon reasonable request.


## References

- Karow, M., Schichor, C., Beckervordersandforth, R. & Berninger, B. Lineage-reprogramming of pericyte-derived cells of the adult human brain into induced neurons. *J. Vis. Exp.* <https://doi.org/10.3791/51433> (2014).
- Yu, P. B. et al. Dorsomorphin inhibits BMP signals required for embryogenesis and iron metabolism. *Nat. Chem. Biol.* **4**, 33–41 (2008).
- Inman, G. J. et al. SB-431542 is a potent and specific inhibitor of transforming growth factor-beta superfamily type I activin receptor-like kinase (ALK) receptors ALK4, ALK5, and ALK7. *Mol. Pharmacol.* **62**, 65–74 (2002).
- Laping, N. J. et al. Inhibition of transforming growth factor (TGF)-beta1-induced extracellular matrix with a novel inhibitor of the TGF-beta type I receptor kinase activity: SB-431542. *Mol. Pharmacol.* **62**, 58–64 (2002).
- Martynoga, B. et al. Epigenomic enhancer annotation reveals a key role for NFIX in neural stem cell quiescence. *Genes Dev.* **27**, 1769–1786 (2013).
- Graham, A. C., Francis-West, P., Brickell, P. & Lumsden, A. The signalling molecule BMP4 mediates apoptosis in the rhombencephalic neural crest. *Nature* **372**, 684–686 (1994).
- Chen, A. E., Borowiak, M., Sherwood, R. I., Khwoudjeu, A. & Melton, D. A. Functional evaluation of ES cell-derived endodermal populations reveals differences between Nodal and Activin A-guided differentiation. *Development* **140**, 675–686 (2013).
- Kumar, A. et al. Nodal signaling uses activin and transforming growth factor-beta receptor-regulated Smads. *J. Biol. Chem.* **276**, 656–661 (2001).
- Schubert, W. Multiple antigen-mapping microscopy of human tissue. in *Experta Medica: Advances in Analytical Cellular Pathology* (eds. Burger, G., Oberholzer, M. & Vooijs, G.P.) 97–98 (Elsevier, Amsterdam, 1990).
- Ferreira, T. A. et al. Neuronal morphometry directly from bitmap images. *Nat. Methods* **11**, 982–984 (2014).
- Schindelin, J. et al. Fiji: an open-source platform for biological-image analysis. *Nat. Methods* **9**, 676–682 (2012).
- Zemankovics et al., 2010
- Trapnell, C., Pachter, L. & Salzberg, S. L. TopHat: discovering splice junctions with RNA-Seq. *Bioinformatics* **25**, 1105–1111 (2009).
- Li, H. et al. The Sequence Alignment/Map format and SAMtools. *Bioinformatics* **25**, 2078–2079 (2009).
- Anders, S., Pyl, P. T. & Huber, W. HTSeq—a Python framework to work with high-throughput sequencing data. *Bioinformatics* **31**, 166–169 (2015).
- Oshlack, A., Robinson, M. D. & Young, M. D. From RNA-seq reads to differential expression results. *Genome Biol.* **11**, 220 (2010).
- Alexa, A., Rahnenführer, J. & Lengauer, T. Improved scoring of functional groups from gene expression data by decorrelating GO graph structure. *Bioinformatics* **22**, 1600–1607 (2006).
- Renaud, G., Kircher, M., Stenzel, U. & Kelso, J. freeBis: an efficient basecaller with calibrated quality scores for Illumina sequencers. *Bioinformatics* **29**, 1208–1209 (2013).

- 724 53. Renaud, G., Stenzel, U., Maricic, T., Wiebe, V. & Kelso, J. deML: robust  
725 demultiplexing of Illumina sequences using a likelihood-based approach.  
726 *Bioinformatics* **31**, 770–772 (2015).
- 727 54. Langmead, B. & Salzberg, S. L. Fast gapped-read alignment with Bowtie 2.  
728 *Nat. Methods* **9**, 357–359 (2012).
- 729
- 730
- 731
- 732
- 733
- 734
- 735
- 736
- 737
- 738
- 739
- 740
- 741
- 742
- 743
- 744
- 745
- 746
- 747
- 748
- 749
- 750
- 751
- 752
- 753
- 754
- 755
- 756
- 757
- 758
- 759
- 760
- 761
- 762
- 763
- 764
- 765
- 766
- 767
- 768
- 769
- 770
- 771
- 772
- 773
- 774
- 775
- 776
- 777
- 778
- 779
- 780
- 781
- 782
- 783
- 784
- 785
- 786
- 787
- 788
- 789
55. Trapnell, C. et al. Transcript assembly and quantification by RNA-Seq reveals  
unannotated transcripts and isoform switching during cell differentiation.  
*Nat. Biotechnol.* **28**, 511–515 (2010).
56. Macosko, E. Z. et al. Highly parallel genome-wide expression profiling of  
individual cells using nanoliter droplets. *Cell* **161**, 1202–1214 (2015).

Uncorrected proofs

# QUERY FORM

<b>Nature Neuroscience</b>	
<b>Manuscript ID</b>	[Art. Id: 168]
<b>Author</b>	Marisa Karow 

**AUTHOR:**

The following queries have arisen during the editing of your manuscript. Please answer by making the requisite corrections directly in the e-proofing tool rather than marking them up on the PDF. This will ensure that your corrections are incorporated accurately and that your paper is published as quickly as possible.

<b>Query No.</b>	<b>Nature of Query</b>
Q1:	Your paper has been copyedited. Please review every sentence to ensure that it conveys your intended meaning; if changes are required, please provide further clarification rather than reverting to the original text. Please note that formatting (including hyphenation and reference citations) has been made consistent with our house style.
Q2:	Author surnames have been highlighted - please check these carefully and indicate if the first name or surname have been marked up incorrectly. Please note that this will affect indexing of your article, such as in PubMed.
Q3:	Please note that the eproof should be amended in only one browser window at any one time, otherwise changes will be overwritten.
Q4:	In the sentence beginning “In sharp contrast, AS...” please provide an exact P value to support this assertion of significance, or revise as “substantial” or similar. The P value may also appear in the supplementary material, but it must appear in the main text.
Q5:	Define violin plot elements, i.e., median, interquartile range, 95% confidence interval, etc.
Q6:	In panel F, define RFU and FSC, and define the blue and purple colors.
Q7:	In D, define ISH
Q8:	In panel B, define P.
Q9:	scRNA correct as defined? Or define scRNA.
Q10:	In the sentence beginning “Cells were first pretreated...” please provide a numerical temperature/temperature range for “room temperature.”
Q11:	The citation “Zemankovics et al., 2010” was moved to the reference list as #46. Please provide sufficient information to identify this paper or remove the reference.
Q12:	iGraph URL okay as updated?
Q13:	Please ensure that this accession code record is released within 1–2 weeks of receiving your eProof.
Q14:	Please confirm that you have provided names and affiliations for all researchers who provided materials.
Q15:	Please check that the Competing Interests declaration is correct as stated. If you declare competing interests, please check the full text of the declaration for accuracy and completeness.
Q16:	Fill out this reference with either: author names, journal name, volume and page number(s) or DOI.



# QUERY FORM

<b>Nature Neuroscience</b>	
<b>Manuscript ID</b>	[Art. Id: 168]
<b>Author</b>	Marisa Karow

**AUTHOR:**

The following queries have arisen during the editing of your manuscript. Please answer by making the requisite corrections directly in the e-proofing tool rather than marking them up on the PDF. This will ensure that your corrections are incorporated accurately and that your paper is published as quickly as possible.

<i>Query No.</i>	<i>Nature of Query</i>
Q17:	Define violin plot elements, i.e., median, interquartile range, 95% confidence interval, etc.

## Reporting Summary

Nature Research wishes to improve the reproducibility of the work that we publish. This form provides structure for consistency and transparency in reporting. For further information on Nature Research policies, see [Authors & Referees](#) and the [Editorial Policy Checklist](#).

### Statistical parameters

When statistical analyses are reported, confirm that the following items are present in the relevant location (e.g. figure legend, table legend, main text, or Methods section).

n/a Confirmed

- The exact sample size ( $n$ ) for each experimental group/condition, given as a discrete number and unit of measurement
- An indication of whether measurements were taken from distinct samples or whether the same sample was measured repeatedly
- The statistical test(s) used AND whether they are one- or two-sided  
*Only common tests should be described solely by name; describe more complex techniques in the Methods section.*
- A description of all covariates tested
- A description of any assumptions or corrections, such as tests of normality and adjustment for multiple comparisons
- A full description of the statistics including central tendency (e.g. means) or other basic estimates (e.g. regression coefficient) AND variation (e.g. standard deviation) or associated estimates of uncertainty (e.g. confidence intervals)
- For null hypothesis testing, the test statistic (e.g.  $F$ ,  $t$ ,  $r$ ) with confidence intervals, effect sizes, degrees of freedom and  $P$  value noted  
*Give  $P$  values as exact values whenever suitable.*
- For Bayesian analysis, information on the choice of priors and Markov chain Monte Carlo settings
- For hierarchical and complex designs, identification of the appropriate level for tests and full reporting of outcomes
- Estimates of effect sizes (e.g. Cohen's  $d$ , Pearson's  $r$ ), indicating how they were calculated
- Clearly defined error bars  
*State explicitly what error bars represent (e.g. SD, SE, CI)*

*Our web collection on [statistics for biologists](#) may be useful.*

### Software and code

Policy information about [availability of computer code](#)

Data collection

For Sholl analyses images were analyzed using the ImageJ(v1.51a-1.51h) Plugin Sholl Analysis v3.6.4; tracing individual neuronal processes was performed using ImageJ software.

Data analysis

Details about data analysis and visualization are provided in the Online Methods section of the paper. The following versions were used: Bioconductor package TopGO v2.3.1 employing the default algorithm weight01, GraphPad Prism v6.01, Igor Pro6 6.0.3.0; Custom R packages were used: TopHat v2.0.8, SAMTOOLS v.0.1.19, HTSeq v0.5.4p1, DESeq2 v1.3.0, FactoMineR v1.34, Seurat v1.4, Monocle2 v2.6.4, igraph v1.2.1, Seurat v2.1-2.2

For manuscripts utilizing custom algorithms or software that are central to the research but not yet described in published literature, software must be made available to editors/reviewers upon request. We strongly encourage code deposition in a community repository (e.g. GitHub). See the Nature Research [guidelines for submitting code & software](#) for further information.

## Data

Policy information about [availability of data](#)

All manuscripts must include a [data availability statement](#). This statement should provide the following information, where applicable:

- Accession codes, unique identifiers, or web links for publicly available datasets
- A list of figures that have associated raw data
- A description of any restrictions on data availability

The scRNA-seq data used in this study have been in the Gene Expression Omnibus (GEO) under accession number GSE113036. The data that support the findings of this study are available from the corresponding author upon reasonable request. Correspondence and requests for materials and data should be addressed to M.K. (marisa.karow@med.uni-muenchen.de), and B.T. (barbara\_treutlein@eva.mpg.de), and B.B. (berningb@uni-mainz.de).

## Field-specific reporting

Please select the best fit for your research. If you are not sure, read the appropriate sections before making your selection.

Life sciences       Behavioural & social sciences       Ecological, evolutionary & environmental sciences

For a reference copy of the document with all sections, see [nature.com/authors/policies/ReportingSummary-flat.pdf](https://www.nature.com/authors/policies/ReportingSummary-flat.pdf)

## Life sciences study design

All studies must disclose on these points even when the disclosure is negative.

Sample size	No statistical methods were used to pre-determine sample sizes but our sample sizes are similar to those reported in previous publications (Karow et al., Cell Stem Cell 2012; Treutlein et al., Nature 2016)
Data exclusions	No data points were excluded for the analysis, except for cells in the scRNA-seq analyses not fulfilling the required criteria. For the fluidigm C1 scRNA-seq data: We excluded cells that had less than 100,000 reads, did not express > 1000 genes, or did not express either of two housekeeping genes ACTB and GAPDH. For the 10x Genomics scRNA-seq data: only single cells with 1,000-7,000 genes were included; cells with lower or higher number of detected genes were excluded.
Replication	For all experiments all replicates are indicated in the figure legends or the methods sections. We have provided all informations to reproduce the experiments. All replications were successful.
Randomization	Samples (pericyte donors, coverslips in 24-well plates, T25 or T75 cell culture flasks) were randomly assigned for transduction with different viruses.
Blinding	scRNA-sequencing analyses were performed unbiasedly and therefore blinding is not applicable. Regarding all other data, if not indicated otherwise (e.g. Sholl analysis), data collection and analysis were not performed blind to the conditions of the experiments. These experiments were performed by a single experimentator (MK)

## Reporting for specific materials, systems and methods

### Materials & experimental systems

n/a	Involvement in the study
<input type="checkbox"/>	<input checked="" type="checkbox"/> Unique biological materials
<input type="checkbox"/>	<input checked="" type="checkbox"/> Antibodies
<input type="checkbox"/>	<input type="checkbox"/> Eukaryotic cell lines
<input type="checkbox"/>	<input type="checkbox"/> Palaeontology
<input type="checkbox"/>	<input type="checkbox"/> Animals and other organisms
<input type="checkbox"/>	<input checked="" type="checkbox"/> Human research participants

### Methods

n/a	Involvement in the study
<input type="checkbox"/>	<input type="checkbox"/> ChIP-seq
<input type="checkbox"/>	<input checked="" type="checkbox"/> Flow cytometry
<input type="checkbox"/>	<input type="checkbox"/> MRI-based neuroimaging

## Unique biological materials

Policy information about [availability of materials](#)

Obtaining unique materials      All unique material (Ascl1/Sox2 encoding viruses) are available from the authors upon



Obtaining unique materials

## Antibodies

Antibodies used

Validation

## Eukaryotic cell lines

Policy information about [cell lines](#)

Cell line source(s)

Authentication

Mycoplasma contamination

Commonly misidentified lines (See [ICLAC](#) register)

## Palaeontology

Specimen provenance

Specimen deposition

Dating methods

Tick this box to confirm that the raw and calibrated dates are available in the paper or in Supplementary Information.

## Animals and other organisms

Policy information about [studies involving animals](#); [ARRIVE guidelines](#) recommended for reporting animal research

Laboratory animals

Wild animals

Field-collected samples

## Human research participants

Policy information about [studies involving human research participants](#)

Population characteristics

Recruitment

## ChIP-seq

Data deposition

- Confirm that both raw and final processed data have been deposited in a public database such as [GEO](#).
- Confirm that you have deposited or provided access to graph files (e.g. BED files) for the called peaks.

Data access links   
*May remain private before publication.*

Files in database submission

Genome browser session (e.g. [UCSC](#))

## Methodology

Replicates	Describe the experimental replicates, specifying number, type and replicate agreement.
Sequencing depth	Describe the sequencing depth for each experiment, providing the total number of reads, uniquely mapped reads, length of reads and whether they were paired- or single-end.
Antibodies	Describe the antibodies used for the ChIP-seq experiments; as applicable, provide supplier name, catalog number, clone name, and lot number.
Peak calling parameters	Specify the command line program and parameters used for read mapping and peak calling, including the ChIP, control and index files used.
Data quality	Describe the methods used to ensure data quality in full detail, including how many peaks are at FDR 5% and above 5-fold enrichment.
Software	Describe the software used to collect and analyze the ChIP-seq data. For custom code that has been deposited into a community repository, provide accession details.

## Flow Cytometry

### Plots

Confirm that:

- The axis labels state the marker and fluorochrome used (e.g. CD4-FITC).
- The axis scales are clearly visible. Include numbers along axes only for bottom left plot of group (a 'group' is an analysis of identical markers).
- All plots are contour plots with outliers or pseudocolor plots.
- A numerical value for number of cells or percentage (with statistics) is provided.

### Methodology

Sample preparation	For sorting of transduced cells for further i) culturing, ii) bulk RNA-sequencing, iii) scRNA-sequencing, primary pericytes were detached from the culture dish using TrypLE for 4-6 minutes and subsequently resuspended in 500-1000 $\mu$ l pericyte growth medium. For the separation of LEPR-positive and -negative pericyte populations, pericyte cultures were detached from the culture dish using TrypLE for 4-6 minutes and subsequently 1-5 x 10 <sup>5</sup> cells were resuspended in 100 $\mu$ l staining solution (PBS plus 0.5% BSA).
Instrument	FACS Aria (BD)
Software	FACS Diva Software
Cell population abundance	The purity of the fluorescent reporter-positive populations that were used for (bulk- and) scRNA-sequencing was confirmed via quantification of the reporter gene expression and resulted in a purity of more than 92%. Due to limitations of using the directly PE conjugated anti-LepR antibody, the purity of the post-sort fraction of the LepR-positive cell population could not be confirmed by additional post-FACS immunohistochemistry.
Gating strategy	For sort of transduced cells: Gating was achieved via subtracting the autofluorescence of non transduced cells and control (DsRed or GFP only) transduced cells were used as respective controls. For the LEPR-based sort: An Alexa647-conjugated isotype control antibody (1:100, BD Pharmingen) was used to gate the proper populations.
<input checked="" type="checkbox"/> Tick this box to confirm that a figure exemplifying the gating strategy is provided in the Supplementary Information.	

## Magnetic resonance imaging

### Experimental design

Design type	no MRI imaging used in this study
Design specifications	Specify the number of blocks, trials or experimental units per session and/or subject, and specify the length of each trial or block (if trials are blocked) and interval between trials.
Behavioral performance measures	State number and/or type of variables recorded (e.g. correct button press, response time) and what statistics were used to establish that the subjects were performing the task as expected (e.g. mean, range, and/or standard deviation across subjects).

## Acquisition

Imaging type(s)

Field strength

Sequence & imaging parameters

Area of acquisition

Diffusion MRI  Used  Not used

## Preprocessing

Preprocessing software

Normalization

Normalization template

Noise and artifact removal

Volume censoring

## Statistical modeling &amp; inference

Model type and settings

Effect(s) tested

Specify type of analysis:  Whole brain  ROI-based  Both

Statistic type for inference (See [Eklund et al. 2016](#))

Correction

## Models &amp; analysis

n/a	Involved in the study
<input type="checkbox"/>	<input type="checkbox"/> Functional and/or effective connectivity
<input type="checkbox"/>	<input type="checkbox"/> Graph analysis
<input type="checkbox"/>	<input type="checkbox"/> Multivariate modeling or predictive analysis

Functional and/or effective connectivity

Graph analysis

Multivariate modeling and predictive analysis